Mon. Not. R. Astron. Soc. **000**, 1–?? (2013) Printed 24 April 2017 (MN LATEX style file v2.2)

Fundamental properties of $Kepler$ and $CoRoT$ targets: IV. Masses and radii from frequencies of minimum $\Delta\nu$ and their implications

M. Yıldız⋆, Z. Çelik Orhan and C. Kayhan
Department of Astronomy and Space Sciences, Science Faculty, Ege University, 35100, Bornova, İzmir, Turkey.

Accepted 2013 May 15. Received 2013 April 11; in original form 2013 April 11

ABSTRACT
Due to the He II ionization zone glitch, the large separation between the oscillation frequencies has an oscillatory component in the spacing of oscillation frequencies and becomes minimum at several reference frequencies ($\nu_{\rm min0}$, $\nu_{\rm min1}$ and $\nu_{\rm min2}$). Recently, by analysing the oscillation frequencies of 90 stars, Yıldız, Çelik Orhan & Kayhan (2016) have shown that these reference frequencies have very strong diagnostic potential for the determination of their effective temperatures. In the present study, we continue to analyse the same stars and compute their mass, radius and age. For most of the stars, the masses computed using $\nu_{\rm min0}$ and $\nu_{\rm min1}$ are very close to each other. For 34 stars, the difference between these masses is less than 0.02 $M_\odot$. The radii of these stars from $\nu_{\rm min0}$ and $\nu_{\rm min1}$ are even closer, with differences of less than 0.007 $R_\odot$. These stars may be the most well known solar-like oscillating stars and deserve to be studied in detail. The asteroseismic expressions we derive for mass and radius show slight dependence on metallicity. We therefore develop a new method for computing initial metallicity from the present surface metallicity by taking into account the effect of microscopic diffusion. The time dependence of initial metallicity shows some very interesting features that may be important for our understanding of chemical enrichment of the galactic disc. According to our findings, every epoch of the disc has its own lowest and highest values for metallicity. While the highest metallicity slowly increased in the past 7 Gyr, the lowest limit increased from 0.006 to 0.020 in the same time interval. We also discuss time dependence of the rotational speeds ($v \sin i$) of these slowly rotating stars. It seems that rotational velocity is inversely proportional to 5/4 power of age rather than 1/2 as given by the Skumanich relation.

Key words: stars: evolution – stars: interiors – stars: late-type – stars: oscillations – stars: fundamental parameters

1 INTRODUCTION

Determining the age of cool stars is crucial for many branches of astrophysics, and precise determination of age from stellar properties primarily depends on how accurately the masses of such stars are calculated. Uncertainty of 10 per cent in mass corresponds to uncertainty of at least 30 per cent in age. The mass (M) and radius (R) of stars can be obtained by asteroseismic methods from the frequency of maximum amplitude ($\nu_{\rm max}$), mean value of the large separation between oscillation frequencies ($\langle\Delta\nu\rangle$), and effective temperature ($T_{\rm eff}$). The relations used in these methods are called scaling relations. In Yıldız, Çelik Orhan & Kayhan (2016; hereafter Paper III), new scaling relations were obtained based on variation of the first adiabatic exponent at stellar surface ($\Gamma_{1\rm s}$). However, for precise M and R determination, new methods are required because, in most cases, in particular $\nu_{\rm max}$ cannot be found very accurately from the power spectrum. Even for the Sun, the uncertainty in $\nu_{\rm max}$ ($\Delta\nu_{\rm max}$) is not small enough. In the literature, the range of solar $\nu_{\rm max}$ is 3021-3150 μHz (see, for example, Stello et al. 2008, Kallinger et al. 2010, Huber et al. 2011, Mathur et al. 2012). The difference is about 4 per cent. Since mass in scaling relation ($M_{\rm sca}$) is proportional to $\nu_{\rm max}^3$, the uncertainty in mass of such a star is very high, about 12 per cent. The uncertainty in frequencies of the minimum $\Delta\nu$, however, is much less than $\Delta\nu_{\rm max}$. Therefore, we want to derive new scaling relations from the MESA models (Paper III) using the new reference frequencies found from the minimum $\Delta\nu$ ($\nu_{\rm min0}$, $\nu_{\rm min1}$ and $\nu_{\rm min2}$).

The oscillatory component of frequency spacings is shaped by the He II ionization zone just below the stellar surface (see, for example, figure 7 in Yıldız et al. 2014a; hereafter Paper I). Many quantities in such outer regions have a very sharp gradient and may be model-dependent. However, excellent results have already been obtained for $T_{\rm eff\odot}$, and for M and R of Procyon A using the new asteroseismic relations. These successful applications motivate us to go further.

In Paper III, we computed the effective temperature of stars

⋆ E-mail: mutlu.yildiz@ege.edu.tr

from purely asteroseismic relations using $\nu_{\rm min0}$, $\nu_{\rm min1}$ and $\nu_{\rm min2}$. There are very clear relations between $T_{\rm eff}$ and the order difference $\Delta n_{\rm xi} = (\nu_{\rm max} - \nu_{\rm min_i})/\Delta\nu$. For some stars, there are systematic differences between asteroseismic and observational $T_{\rm eff}$s (spectroscopic and photometric). In such cases, we can modify the value of $\nu_{\rm max}$ so that all three quantities $T_{\rm eff}$, $M_{\rm sca}$ and radius from scaling relations ($R_{\rm sca}$) are in good agreement with the values obtained in other ways (asteroseismic and non-asteroseismic).

In the present study, we analyze observed oscillation frequencies, check the relations between the reference frequencies, and apply the new methods to the $Kepler$ and $CoRoT$ target stars. We find their M, $T_{\rm eff}$, R, luminosity (L), age ($t_{\rm sis}$), and distance ($d_{\rm sis}$) using asteroseismic parameters. The role of the small separation between oscillation frequencies ($\delta\nu_{02}$) is crucial in the computation of $t_{\rm sis}$ for main-sequence (MS) stars. Its mean value ($\langle\delta\nu_{02}\rangle$) is about 15 μHz for zero-age MS stars and 5 μHz for terminal-age MS (TAMS) stars.

This paper is organized as follows. In Section 2, we develop new asteroseismic methods for the computation of R, surface gravity (g), M and $t_{\rm sis}$ in terms of asteroseismic quantities. Some of these methods slightly depend on metallicity (Z). Therefore, Section 3 is devoted to finding initial metallicity ($Z_{\rm o}$) from the present surface metallicity ($Z_{\rm s}$) by taking into account the effect of microscopic diffusion. In Section 4, we present the results obtained from applications of the methods developed in Sections 2 and 3 to the $Kepler$ and $CoRoT$ targets, and to some stars observed by ground-based telescopes. The consequences of our findings in regards to the chemical evolution of the galactic disc and gyrochronology are presented in Section 5. Finally, we draw our conclusions in Section 6.

2 NEW SCALING RELATIONS FROM THE INTERIOR MODELS USING THE MESA CODE

The models used in the analysis of the present study are the same as those in Paper III. The details of the models constructed by using the MESA code (Paxton et al. 2011) are given there. The symbols used in the present study have the same meaning as in Paper III.

2.1 Scaling relations in terms of $\nu_{\rm min1}$, $\langle\Delta\nu\rangle$ and $T_{\rm eff}$

In some cases, $\nu_{\rm max}$ either cannot be determined from the observed data or its uncertainty is not low enough for accurate determination of stellar M and R. Therefore, using the MESA models with solar (initial) metallicity ($Z_\odot = 0.0172$), we also derive new relations using $\nu_{\rm min0}$, $\nu_{\rm min1}$ and $\nu_{\rm min2}$ in place of $\nu_{\rm max}$. For radius ($R_{\rm sis1}$) in terms of $\nu_{\rm min1}$, $\langle\Delta\nu\rangle$ and $T_{\rm eff}$, we derive the fitting formula as

$$\frac{R_{\rm sis1}}{R_\odot} = \frac{\left(\frac{\nu_{\rm min1}}{\nu_{\rm min1\odot}}\right)^{0.156}\left(\frac{\langle\Delta\nu_\odot\rangle}{\langle\Delta\nu\rangle}\right)^{0.92}}{(1.14(r_{T\Gamma}-1.11)^2+0.98)(-0.64r_{\delta\Delta}+1.05)}, \quad (1)$$

where

$$r_{T\Gamma} = \frac{T_{\rm eff}}{T_{\rm eff\odot}}\frac{\Gamma_{\rm 1s\odot}}{\Gamma_{\rm 1s}}, \quad (2)$$

and

$$r_{\delta\Delta} = \frac{\langle\delta\nu_{02}\rangle}{\langle\Delta\nu\rangle}. \quad (3)$$

$R_{\rm sis1}$ is plotted with respect to model radius ($R_{\rm mod}$) in Fig. 1. The maximum difference between equation (1) and $R_{\rm mod}$ is about 1 per cent.

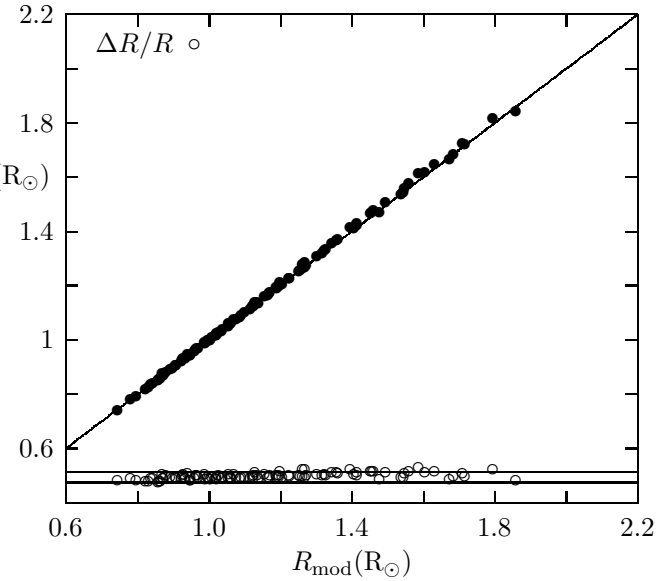

Figure 1. Radius computed from asteroseismic data is plotted with respect to model radius (filled circles). The circles represent the fractional difference between these radii. Most of the circles lie between the two horizontal lines for 0.01 and -0.01. This implies that uncertainty is about 1 per cent.

Similarly, we also derive an expression for asteroseismic gravity ($g_{\rm sis1}$) for the solar metallicity:

$$\frac{g_{\rm sis1}}{g_\odot} = \frac{\left(\frac{\nu_{\rm min1}}{\nu_{\rm min1\odot}}\frac{\langle\Delta\nu\rangle}{\langle\Delta\nu_\odot\rangle}\right)^{0.58}}{(1.6(r_{T\Gamma}-1.06)^2+0.992)}. \quad (4)$$

$g_{\rm sis1}$ is plotted with respect to model gravity ($g_{\rm mod}$) in Fig. 2. The maximum difference between equation (4) and model gravity is about 2 per cent.

For stellar mass from min1, we compute $M_{\rm sis1}$ from $g_{\rm sis1}$ and $R_{\rm sis1}$: $M_{\rm sis1}/M_\odot = (g_{\rm sis1}/g_\odot)(R_{\rm sis1}/R_\odot)^2$. From the MESA models, there is a relation between $\nu_{\rm min0}$ and $\nu_{\rm min1}$:

$$\left(\frac{\nu_{\rm min1}}{\nu_{\rm min1\odot}}\right) = \left(\frac{\nu_{\rm min0}}{\nu_{\rm min0\odot}}\right)^{1.042}. \quad (5)$$

By inserting equation (5) in equations (1) and (4), we obtain expressions for radius ($R_{\rm sis0}$) and gravity ($g_{\rm sis0}$) in terms of $\nu_{\rm min0}$, respectively. Again, we follow the same steps for computation of $M_{\rm sis0}$ as for $M_{\rm sis1}$.

$\Gamma_{\rm 1s\odot}$ is taken as 1.639. The other solar quantities used in our methods are given at the end of Table A1.

2.2 Effects of metallicity on the scaling relations

Models with different metallicities show that there is a slight dependence on Z, which can be important for a precise determination of R and other basic stellar parameters. We obtain

$$\frac{R_{\rm sis1}(Z)}{R_{\rm sis1}(Z=Z_\odot)} = \left(\frac{Z}{Z_\odot}\right)^{0.06}. \quad (6)$$

For gravity with arbitrary Z,

$$\frac{g_{\rm sis1}(Z)}{g_{\rm sis1}(Z=Z_\odot)} = \left(\frac{Z}{Z_\odot}\right)^{0.025} \quad (7)$$

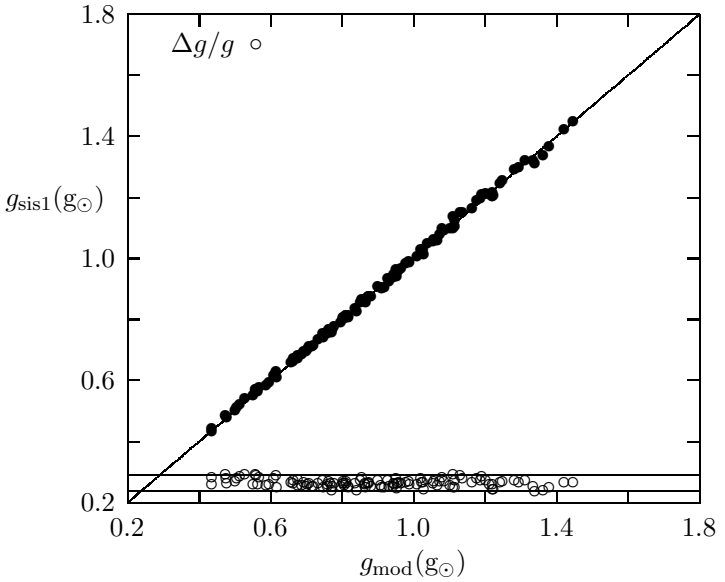

Figure 2. Gravity at the surface computed from asteroseismic data is plotted with respect to model gravity (filled circles). The circles represent the fractional difference between these gravities. Most of the circles lie between the two horizontal lines for 0.02 and -0.02. This implies that typical uncertainty is about 2 per cent.

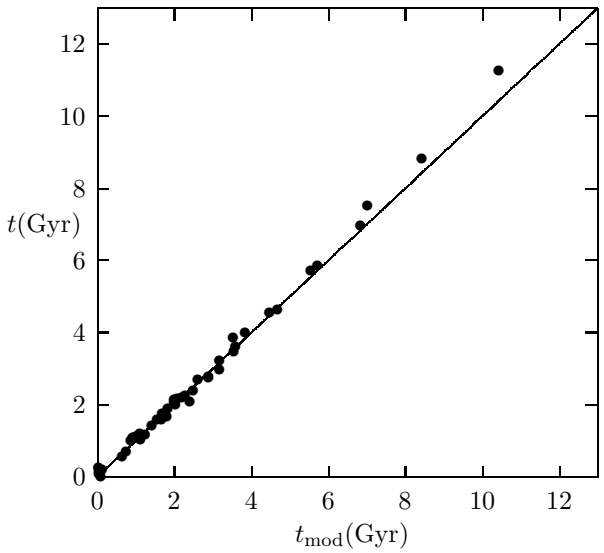

Figure 3. Age derived from oscillation frequencies (equation 8) with respect to model age. Mass range is 0.9-1.6 $\rm M_\odot$. The agreement between the two ages is very good, particularly for ages less than 7 Gyr.

is derived. Indeed, equations (6) and (7) show that both $R_{\rm sis1}$ and $g_{\rm sis1}$ slightly depend on Z, respectively. For example, if $Z = 2Z_\odot$, $R_{\rm sis1}(Z)$ and $g_{\rm sis1}(Z)$ are only 4 and 2 per cent greater than their values with solar metallicity, respectively. However, as long as we deal with fundamental parameters such as mass and radius, such a level of precision is important.

We do the same computations for min0 and obtain $g_{\rm sis0}(Z)$, $R_{\rm sis0}(Z)$ and $M_{\rm sis0}(Z)$ (see Table A1).

2.3 Computation of age

For the MESA models with mass ranging from 0.8 to 1.6 $\rm M_\odot$, we derive a fitting formula for $t_{\rm sis}$ in terms of $\langle\delta\nu_{02}\rangle$, M and Z as

$$t_{\rm sis}(\rm Gyr) = \frac{a_t(Z)\,\langle\delta\nu_{02}\rangle\,/\,\langle\delta\nu_{02\odot}\rangle\,(M/\rm M_\odot)^{1.2} + b_t(Z)}{(M/\rm M_\odot)^{n_t(Z)}} \quad (8)$$

where

$$a_t(Z) = 9.84(0.931\left(\frac{Z_\odot}{Z} - 0.331\right)^{0.2} - 1.627), \quad (9)$$

$$b_t(Z) = 6.176\left(\frac{Z}{Z_\odot}\right) + 6.016 \quad (10)$$

and

$$n_t(Z) = -0.2447\left(\frac{Z_\odot}{Z}\right) + 3.3848. \quad (11)$$

$n_t(Z)$ is the slope obtained from the graph of $\log(t)$ with respect to $\log(M)$.

$\langle\delta\nu_{02}\rangle$ (or $\langle\delta\nu_{02}\rangle\,/\,\langle\delta\nu_{02\odot}\rangle$) is considered the best age indicator of a star; however, it actually represents relative age in MS. Relative age can be defined as the age in units of TAMS age, which strongly depends on stellar mass and metallicity. Therefore, in order to find absolute age, stellar mass and metallicity must be precisely obtained from observations. $t_{\rm sis}$ found from equation (8) is plotted with respect to model age in Fig. 3. They are in very good agreement, especially for ages less than 7 Gyr.

We also compute age using the method developed by Yıldız et al. (2014b) for the planet-candidate host stars. This method is based on the observed M, R and Z values of a star. This age ($t_{\rm yil}$) and age ($t_{\rm sis}$) from equation (8) are listed in Table A1.

If a star is a post-MS star, then we take its age as its TAMS age. $\langle\delta\nu_{02}\rangle$ is already an age indicator for MS stars.

2.4 Uncertainties in radius, gravity, mass and age

From equation (1), the typical uncertainty ($\Delta R_{\rm sis1}$) in $R_{\rm sis1}$ is derived as

$$\frac{\Delta R_{\rm sis1}}{R_{\rm sis1}} = 0.156\frac{\Delta\nu_{\rm min1}}{\nu_{\rm min1}} + 0.92\frac{\Delta\,\langle\Delta\nu\rangle}{\langle\Delta\nu\rangle}. \quad (12)$$

Similarly, uncertainty in gravity ($\Delta g_{\rm sis1}$) is obtained as

$$\frac{\Delta g_{\rm sis1}}{g_{\rm sis1}} = 0.58\frac{\Delta\nu_{\rm min1}}{\nu_{\rm min1}} + 0.58\frac{\Delta\,\langle\Delta\nu\rangle}{\langle\Delta\nu\rangle} \quad (13)$$

using equation (4).

Since we compute mass by multiplying the square of equation (1) by equation (4), it can be shown that the typical uncertainty in mass is given as

$$\frac{\Delta M_{\rm sis1}}{M_{\rm sis1}} = 0.89\frac{\Delta\nu_{\rm min1}}{\nu_{\rm min1}} + 1.26\frac{\Delta\,\langle\Delta\nu\rangle}{\langle\Delta\nu\rangle}. \quad (14)$$

For $M_{\rm sis0}$, $R_{\rm sis0}$ and $g_{\rm sis0}$ we use the same methods but $\Delta\nu_{\rm min0}/\nu_{\rm min0}$ is employed in place of $\Delta\nu_{\rm min1}/\nu_{\rm min1}$.

3 COMPUTATION OF INITIAL METALLICITY FROM PRESENT SURFACE METALLICITY AND MICROSCOPIC DIFFUSION

From comparison of solar models with the helioseismic inferences, such as sound speed, bottom radius of the convective zone (CZ), and surface helium abundance, one can expect that microscopic diffusion works throughout the radiative interior and ultimately affects the composition of the solar CZ and photosphere (Michaud & Proffitt 1993; Thoul, Bahcall & Loeb 1994; Bahcall, Serenelli & Pinsonneault 2004; Yıldız 2011). Further confirmation can perhaps be carried out in clusters, particularly old open clusters. In at least two clusters, there are strong indicators that diffusion works (see below).

It is well known that rotation causes mixing and therefore prevents diffusion of chemical species. MS stars with convective envelopes are slow rotators and therefore one can observe the influence of diffusion in these stars. However, the efficiency of diffusion also depends on the depth of CZ. The shallower the CZ is, the faster the diffusion velocity at the bottom of CZ is. Therefore, there must be a metallicity gradient along the MS of an old cluster. Metallicity is minimum at the turn-off (TO) and increases toward the cool side of MS. As stars evolve away from MS, CZ deepens and mixes the outer and inner regions. Therefore, near the red giant branch (RGB), the metallicity at the surface is approximately the same as initial metallicity. The metallicity difference between RGB and TO is found as 0.08 dex for NGC 6752 (Gruyters, Nordlander & Korn 2014), 0.16 dex for NGC 6397 (Korn et al. 2007), 0.25 dex for M30 (Gruyters et al. 2016) and 0.26 dex for M92 (King et al. 1998).

3.1 Surface and initial metallicities

We have computed metallicity of the stars from the [Fe/H] values derived from spectroscopic studies (Bruntt et al. 2012; Molenda-Żakowicz et al. 2013). As in the case of Yıldız et al. (2014b), we compute [O/H] value using the relation between [O/H] and [Fe/H] abundances in the solar-neighbourhood (Edvardsson et al. 1993) and obtain Z from the relation

$$Z = 10^{[\mathrm{O/H}]} Z_{\odot}. \quad (15)$$

This metallicity is the metallicity in the photospheres of the stars ($Z_{\rm s}$). However, we want to find the initial metallicity ($Z_{\rm o}$).

Since metallicity has a slight effect on the scaling relations for radius and gravity (and hence mass), the initial metallicity must be estimated from present surface value and microscopic diffusion velocity.

3.2 Effect of diffusion on surface metallicity of MS stars

The surface metallicity and helium abundance of a slowly rotating cool star decrease during its MS evolution. The difference (δZ) between $Z_{\rm o}$ and $Z_{\rm s}$ is a function of both age and mass of stars. From the ANKİ models of Yıldız, Çelik Orhan & Kayhan (2015; hereafter Paper II) with different mass and metallicity, we find the difference (δZ) between $Z_{\rm o}$ and $Z_{\rm s}$ as

$$\delta Z = Z_{\rm o} - Z_{\rm s} = 5.69 \times 10^{-4}((M/\mathrm{M}_{\odot})^{6.73} + 0.7) t_9^{0.9} \quad (16)$$

where t_9 is $t/10^9$ yr. Microscopic diffusion causes a decrease in the photospheric metallicity of a star relative to its age and mass.

3.3 Effect of deepening CZ on surface metallicity of post-MS stars

The surface metallicity of a cool star increases after its MS phase because deepening CZ mixes low-metallicity outer regions with the metal-rich inner regions. Such a differentiation in metallicity is thought to be caused by microscopic diffusion. For post-MS stars, we introduce a parameter as

$$x_{gT} = \frac{T_{\rm eff}}{\mathrm{T}_{\rm eff\odot}} \log g - 3.35. \quad (17)$$

If $x_{gT} < 0$, then $Z_{\rm o} = Z_{\rm s}/1.06$. If $x_{gT} > 0$,

$$Z_{\rm o} = \frac{Z_{\rm s}}{1 - 0.526 x_{gT}}. \quad (18)$$

4 RESULTS AND DISCUSSIONS

The basic properties of the *Kepler* and *CoRoT* targets are listed in Table A1. The observational properties we use are the same as those given in Paper III. In the present study we compute fundamental properties using methods based in particular on $\nu_{\rm min0}$ and $\nu_{\rm min1}$ rather than $\nu_{\rm max}$, because $\nu_{\rm max}$ is not always precisely determined from the power spectrum (Arentoft et al. 2008). If the parameters obtained by using $\nu_{\rm min0}$ and $\nu_{\rm min1}$ are consistent, then we can slightly modify only $\nu_{\rm max}$ by comparing values of $T_{\rm eff}$, M and R found by using different methods (see Section 4.2).

4.1 Mass, radius, distance and age of the target stars

In Fig. 4, $R_{\rm sis1}$ computed from min1 (equation 1 and 6) is plotted with respect to $R_{\rm sis0}$ from min0. The agreement between these radii seems excellent. The difference between $R_{\rm sis1}$ and $R_{\rm sis0}$ is less than 1 per cent. Such a level of accuracy is achieved for the first time and reflects the diagnostic potential of new reference frequencies $\nu_{\rm min0}$, $\nu_{\rm min1}$ and $\nu_{\rm min2}$.

For $M_{\rm sis1}$, we first compute $g_{\rm sis1}$ from equation (4) and (7) and then multiply it by $R^2_{\rm sis1}$. In a similar way, we obtain $M_{\rm sis0}$ using $\nu_{\rm min0}$ in place of $\nu_{\rm min1}$. In Fig. 5, $M_{\rm sis1}$ is plotted with respect to $M_{\rm sis0}$. The agreement between these masses is amazing. The maximum difference between them is about 4 per cent. However, for 34 stars (including the Sun), the mass difference (δM_{01}) between $M_{\rm sis1}$ and $M_{\rm sis0}$ is less than 0.02 $\mathrm{M}_{\odot}$. These stars are listed in Table 1. The difference between $R_{\rm sis1}$ and $R_{\rm sis0}$ (δR_{01}) is given in the ninth column. The maximum value of δR_{01} is about 0.007 $\mathrm{R}_{\odot}$ for KIC 11717120, the percentage difference is 0.3. These solar-like oscillating stars may be the most well known stars. Their interior models must be studied in detail. Two of these stars, KIC 7871531 and KIC 8760414, have mass low enough to discuss non-ideal effects in the stellar interior. Their masses are calculated as 0.81 and 0.83 $\mathrm{M}_{\odot}$, respectively.

The masses of two stars are already well known from non-asteroseismic observational methods. They are the Sun and Procyon A. Both $M_{\rm sis1}$ and $M_{\rm sis0}$ are 0.99 $\mathrm{M}_{\odot}$ for the Sun. For Procyon A, $M_{\rm sis1} = 1.47$ $\mathrm{M}_{\odot}$ while its mass was determined to be 1.478 $\mathrm{M}_{\odot} \pm 0.012$ from the astrometric data of the *Hubble Space Telescope* (Bond et al. 2015). These results show that the masses found by using the new reference frequencies $\nu_{\rm min0}$ and $\nu_{\rm min1}$ are very accurate.

Much more precise values are derived for radius. For the Sun, for example, both $R_{\rm sis1}$ and $R_{\rm sis0}$ are 0.99 $\mathrm{R}_{\odot}$. There is also satisfactory agreement between the radii of Procyon A determined using asteroseismic and non-asteroseismic methods (see below).

Table 1. The most precise data for the solar-like oscillating stars: $\delta M_{01} =\mid M_{\rm sis0} - M_{\rm sis1} \mid < 0.02$ M$_\odot$and $\delta R_{01} =\mid R_{\rm sis0} - R_{\rm sis1} \mid < 0.007$ R$_\odot$. For Procyon A, δM is the difference between $M_{\rm sis1}$ and $M_{\rm sca}$

Star	$M_{\rm sca}$ M$_\odot$	$M_{\rm sis0}$ M$_\odot$	$M_{\rm sis1}$ M$_\odot$	δM_{01} M$_\odot$	$R_{\rm sca}$ R$_\odot$	$R_{\rm sis0}$ R$_\odot$	$R_{\rm sis1}$ R$_\odot$	δR_{01} R$_\odot$	$Z_{\rm s}$	Z_0
3632418	1.27	1.27	1.29	0.019	1.85	1.84	1.85	0.005	0.0107	0.0171
5607242	1.18	1.15	1.14	0.012	2.37	2.39	2.38	0.004	—	—
5866724	1.25	1.25	1.25	0.000	1.41	1.42	1.42	0.000	0.0164	0.0230
5955122	1.24	1.22	1.24	0.012	2.10	2.14	2.14	0.004	0.0126	0.0192
6116048	1.03	1.03	1.03	0.005	1.23	1.23	1.23	0.001	0.0101	0.0150
6933899	1.17	1.16	1.17	0.007	1.61	1.61	1.62	0.002	0.0141	0.0225
7206837	1.38	1.39	1.38	0.009	1.59	1.59	1.58	0.002	0.0158	0.0240
7747078	1.16	1.13	1.15	0.020	1.96	1.96	1.97	0.006	0.0098	0.0145
7871531	0.81	0.82	0.81	0.005	0.87	0.87	0.87	0.001	0.0101	0.0135
8228742	1.26	1.26	1.26	0.005	1.82	1.82	1.82	0.001	0.0114	0.0182
8379927	1.12	1.11	1.12	0.015	1.12	1.12	1.12	0.003	0.0129	0.0153
8524425	1.13	1.09	1.07	0.017	1.81	1.82	1.82	0.005	0.0158	0.0218
8694723	1.12	1.12	1.11	0.005	1.53	1.54	1.54	0.001	0.0080	0.0128
8760414	0.83	0.83	0.83	0.001	1.04	1.03	1.03	0.000	0.0042	0.0061
9025370	1.00	1.00	1.00	0.002	1.01	1.01	1.01	0.000	0.0136	0.0175
9098294	0.99	0.99	1.00	0.006	1.16	1.15	1.15	0.001	0.0103	0.0152
9410862	1.07	1.07	1.07	0.007	1.20	1.20	1.20	0.001	—	—
9812850	1.29	1.29	1.27	0.013	1.76	1.75	1.75	0.003	0.0103	0.0165
10018963	1.26	1.25	1.24	0.016	1.96	1.97	1.97	0.004	0.0097	0.0155
10454113	1.18	1.18	1.18	0.002	1.26	1.25	1.25	0.000	0.0125	0.0165
10920273	1.20	1.11	1.11	0.000	1.90	1.87	1.87	0.000	0.0131	0.0186
11026764	1.33	1.14	1.13	0.009	2.14	2.06	2.06	0.003	0.0142	0.0191
11244118	1.33	1.20	1.21	0.009	1.69	1.65	1.65	0.002	0.0175	0.0280
11253226	1.63	1.38	1.40	0.020	1.70	1.58	1.58	0.004	0.0106	0.0169
11414712	1.11	1.09	1.11	0.016	2.20	2.23	2.24	0.006	0.0126	0.0155
11717120	0.99	0.87	0.88	0.015	2.33	2.32	2.33	0.007	0.0093	0.0088
11771760	1.81	1.47	1.46	0.004	3.16	2.97	2.97	0.001	—	—
12009504	1.14	1.13	1.14	0.012	1.39	1.39	1.39	0.003	0.0114	0.0170
12069424	1.05	1.04	1.05	0.005	1.22	1.22	1.22	0.001	0.0152	0.0209
12258514	1.21	1.21	1.19	0.017	1.59	1.59	1.58	0.004	0.0141	0.0225
2151	1.10	1.11	1.11	0.001	1.83	1.87	1.87	0.000	0.0119	0.0176
43587	1.08	1.07	1.09	0.019	1.20	1.20	1.20	0.004	0.0131	0.0187
49385	1.27	1.26	1.27	0.018	1.94	1.96	1.97	0.005	0.0149	0.0239
Procyon A	1.48	—	1.47	0.011	2.04	—	2.01	—	0.0134	0.0215
$\odot$	1.00	0.99	0.99	0.000	1.00	0.99	0.99	0.000	0.0134	0.0167

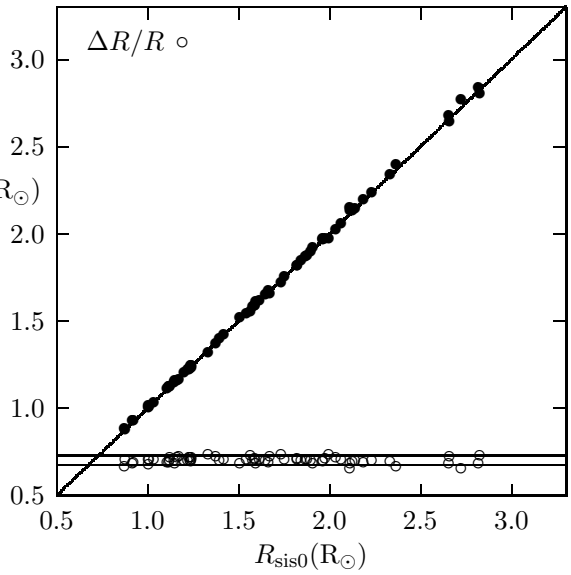

Figure 4. $R_{\rm sis1}$ is plotted with respect to $R_{\rm sis0}$. The horizontal lines represent 0.01 and -0.01 for the uncertainties in radius.

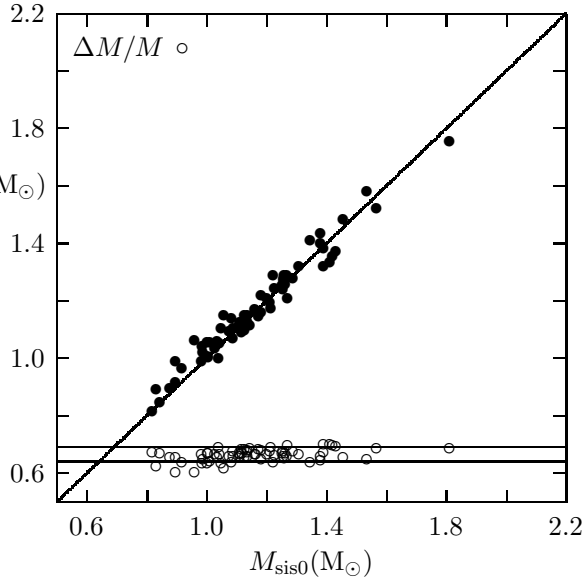

Figure 5. $M_{\rm sis1}$ is plotted with respect to $M_{\rm sis0}$. The horizontal lines represent 0.04 and -0.04 for the uncertainties in mass.

Age is computed from asteroseismic quantities using equation (8). The age ranges from 1.1 to 10 Gyr. We also compute age using the method derived by Yıldız et al. (2014b) for planet-candidate host stars.

4.2 Effective temperature difference between asteroseismic and non-asteroseismic methods and modification in $\nu_{\rm max}$

In Papers I and III, it is shown that $T_{\rm eff}$ is a function of order difference between the minima in $\Delta\nu$ versus ν graph and $\nu_{\rm max}$. Using equations (15)-(17) of Paper III, $T_{\rm eff}$s of the stars are computed by using their $\nu_{\rm min0}$, $\nu_{\rm min1}$ and $\nu_{\rm min2}$ together with $\nu_{\rm max}$ and $\Delta\nu$. For most of the stars, $T_{\rm eff}$s are available from spectroscopic observations and also from colours ($B-V$ and $V-K$). There is in general a very good agreement between these $T_{\rm eff}$s. However, in some cases there is a systematic difference between the $T_{\rm eff}$ values derived from asteroseismic and non-asteroseismic methods. This can be caused by values of $\nu_{\rm max}$, which is perhaps the most uncertain asteroseismic quantity. Therefore, we slightly modify the $\nu_{\rm max}$ value to determine whether the systematic difference can be eliminated. At the same time, we test if mass and radius computed from new scaling relations (Paper III) are improved in comparison with the values obtained using asteroseismic methods based on the frequencies of minimum $\Delta\nu$.

In many cases, the resultant $T_{\rm eff}$, $M_{\rm sca}$ and $R_{\rm sca}$ from the modified scaling relations (equations 9 and 10 in Paper III) come to close to the values ($M_{\rm sis1}$ and $R_{\rm sis1}$) from alternative scaling relations from minima (equations 1 and 4). In Fig. 6 and 7, $M_{\rm sis1}$ and $R_{\rm sis1}$ are plotted with respect to $M_{\rm sca}$ and $R_{\rm sca}$, respectively.

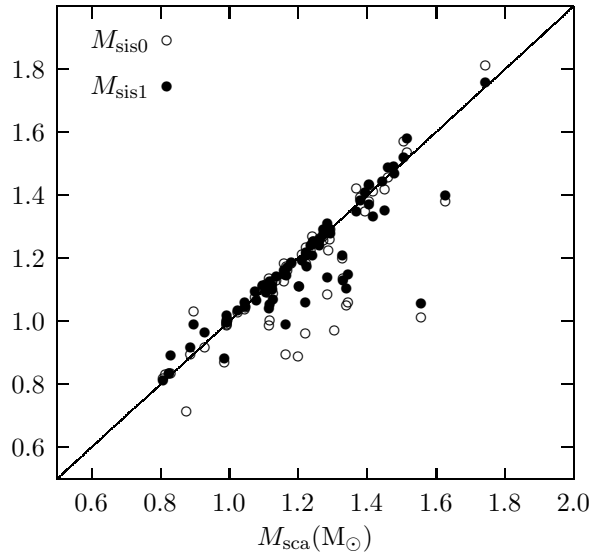

Figure 6. $M_{\rm sis0}$ (circles) and $M_{\rm sis1}$ (filled circles) are plotted with respect to $M_{\rm sca}$.

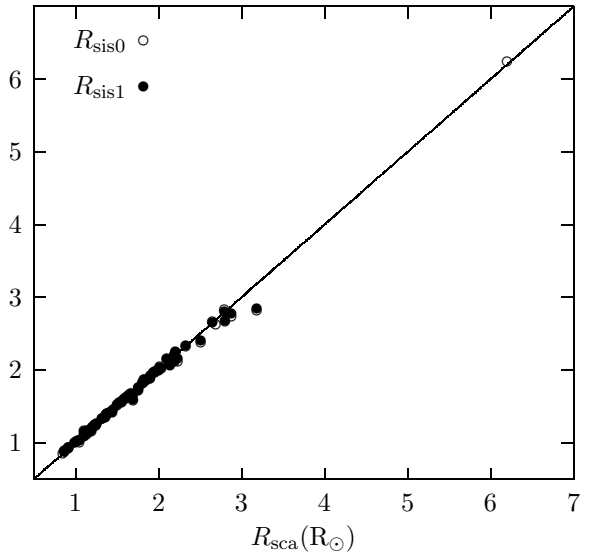

Figure 7. $R_{\rm sis0}$ (circles) and $R_{\rm sis1}$ (filled circles) are plotted with respect to $R_{\rm sca}$.

4.3 Notes on individual stars

Comparison of asteroseismic and GAIA distances (Gaia Collaboration et al. 2016) of individual stars is a useful way to test the methods we have developed. Asteroseismic distance of the targets is computed by applying the same method as in Yıldız et al. (2017). For computation of luminosity, we use radius found from scaling relation with modified $\nu_{\rm max}$ and $T_{\rm eS}$. The GAIA and asteroseismic distances are listed in Table A1. For five of the targets, GAIA parallax is not available. Their distances are computed from HIPPARCOS (Perrymann et al. 1997) parallax (HD 2151, 7.46±0.01 pc; HD 43587, 19.25±0.15 pc; HD 146233, 13.90±0.07 pc; HD 203608, 9.26±0.02 pc; Procyon A, 3.51±0.02 pc).

4.3.1 KIC 3424541

KIC 3424541 is a sub-giant star. Two minima are seen on its $\Delta\nu$ versus ν diagram. It shows mixed modes in its observed oscillation frequencies. Although there is a systematic difference between asteroseismic and non-asteroseismic $T_{\rm eff}$s, for such hot solar-like oscillating stars, asteroseismic $T_{\rm eff}$ is only slightly dependent on the value of $\nu_{\rm max}$. However, if we take $\nu_{\rm max} = 731$ μHz, $R_{\rm sca}$ is in very good agreement with $R_{\rm sis0}$ and $R_{\rm sis1}$, and $M_{\rm sca}$ becomes very close to $M_{\rm sis1}$.

4.3.2 KIC 3427720

Effective temperatures derived from min1 and min0 of KIC 3427720 are lower than both photometric and spectral $T_{\rm eff}$s if we use literature $\nu_{\rm max}$. Decreasing $\nu_{\rm max}$ may remove this systematic difference. If we take $\nu_{\rm max} = 2638$ μHz, then one can obtain a very good agreement between asteroseismic and conventional $T_{\rm eff}$s. Furthermore, the modified $\nu_{\rm max}$ makes $M_{\rm sca}$ and $R_{\rm sca}$ in perfect agreement with the literature values. For example, while $M_{\rm sca}$ with the observed $\nu_{\rm max}$, 1.27 $\rm M_\odot$, is significantly greater than $M_{\rm lit}$ = 1.13 $\rm M_\odot$, $M_{\rm sca}$ with the modified $\nu_{\rm max}$ (1.11 $\rm M_\odot$) is in very good agreement with $M_{\rm lit}$.

4.3.3 KIC 3544595

It is one of the brightest *Kepler* targets and a planet host star with two planets (Ballard et al. 2014). If $\nu_{\rm max}$ is taken as 3226 μHz, the masses, radii and $T_{\rm eff}$s computed with different methods are in much better agreement in comparison to the case with the observed value of $\nu_{\rm max} = 3366$ μHz.

4.3.4 KIC 3632418

The F-like oscillating star KIC 3632418 has a rocky planet (Howell et al. 2012). On the $\Delta\nu$ versus ν diagram of KIC 3632418, it is quite difficult to decide on the minima. If we plot for degrees $l = 0$, $l = 1$, and $l = 2$ on the $\Delta\nu$ versus ν diagram of KIC 3632418, min1 is not confirmed clearly from the data of all degrees. For degree $l = 0$, there is a bump-like structure in the vicinity of min1, and min0 is not seen due to lack of data. Therefore, we determine the min1 and min0 from $l = 1$. If we use the observed value of $\nu_{\rm max} = 1159$ μHz in scaling relations, asteroseismic $T_{\rm eff}$s are slightly different from conventional $T_{\rm eff}$s. However, if we take $\nu_{\rm max} = 1100$ μHz, the agreement between the radii from different methods is improved. The differences between masses, then, are less than 0.02 $\rm M_\odot$.

4.3.5 KIC 3656476

The observed oscillation frequencies of *Kepler* target KIC 3656476 do not allow computation of the frequency of any minima. Therefore, we cannot obtain $T_{\rm sis0}$ and $T_{\rm sis1}$ for this star. $\nu_{\rm max}$ and $\Delta\nu$ are available in the literature. We evaluate mass and radius using the scaling relations. The differences $\Delta M = |M_{\rm sca} - M_{\rm lit}|$ and $\Delta R = |R_{\rm sca} - R_{\rm lit}|$ are small.

4.3.6 KIC 3733735

Its $T_{\rm eS}$ is in good agreement with its $T_{\rm eVK}$. It is one of the stars with known distance. The distance of KIC 3733735 is 104.29 pc. min0

cannot be determined from observed frequencies, but this star has min2 and min1. We can compute effective temperatures, masses, and radii from $\nu_{\rm min1}$ and $\nu_{\rm min2}$. If we increase $\nu_{\rm max}$ by about 27 μHz, $M_{\rm sca}$ and $R_{\rm sca}$ are in very good agreement with $M_{\rm sis1}$ and $R_{\rm sis1}$, respectively.

4.3.7 KIC 4349452

KIC 4349452 has three planets. Two of these planets are Neptune-sized (Benomar et al. 2014). If we reduce the observed $\nu_{\rm max}$ by only 46 μHz, $T_{\rm sis0}$ and $T_{\rm sis1}$ are in much better agreement with $T_{\rm eS}$. $R_{\rm sca}$ with modified $\nu_{\rm max}$, $R_{\rm sis0}$ and $R_{\rm sis1}$ are very close to each other.

4.3.8 KIC 4914923

KIC 4914923 is a high proper motion star. Neilsen et al. (2015) have identified rotational splitting of its p-mode frequencies. The rotation period of KIC 4914923 is determined as 1.23 ± 0.29 in unit of solar rotation period.

The observed $\nu_{\rm max}$ of KIC 4914923 is given as 1849 μHz. From its oscillation frequencies, we find $\nu_{\rm min0}$ as 1947.8 μHz. The difference between $T_{\rm eS}$ and $T_{\rm sis0}$ is about 173 K. While $R_{\rm sis0}$ and $R_{\rm lit}$ are as 1.38 and 1.37 $R_\odot$, this value of $\nu_{\rm max}$ yields $R_{\rm sca} = 1.43$ $R_\odot$. If we reduce $\nu_{\rm max}$ to 1775 μHz, the difference between $T_{\rm eS}$ and $T_{\rm sis0}$ becomes only 35 K and $R_{\rm sca}$ is found as 1.37 $R_\odot$, in much better agreement with $R_{\rm sis0}$ and $R_{\rm lit}$. $M_{\rm sis0}$, $M_{\rm lit}$ and $M_{\rm sca}$ with modified $\nu_{\rm max}$ are all equal to 1.10 $M_\odot$.

4.3.9 KIC 5184732

$\nu_{\rm min0}$ and $\nu_{\rm min1}$ of KIC 5184732 are determined from observed oscillation frequencies of modes with $l = 1$. Half of min1 is seen in the $\Delta\nu$ versus ν graph, which implies that the assigned value for $\nu_{\rm min1}$ (1705.5 μHz) can be considered the upper limit. Its $T_{\rm eVK}$ is in excellent agreement with $T_{\rm eS}$. The observed value of $\nu_{\rm max}$ (2068 μHz) gives $T_{\rm sis0}$ as 180 K less than $T_{\rm eS}$. We notice that $M_{\rm sca}$ and $R_{\rm sca}$ are greater than $M_{\rm sis0}$ and $R_{\rm sis0}$, respectively. These systematic differences can be eliminated by modifying the value of $\nu_{\rm max}$. If $\nu_{\rm max}$ is taken as 1988 μHz, $T_{\rm sis0} = T_{\rm eS}$. However, $\nu_{\rm max} = 1978$ μHz makes $M_{\rm sca}$ and $R_{\rm sca}$ in very good agreement with $M_{\rm sis0}$ and $R_{\rm sis0}$, respectively, and the difference between $T_{\rm sis0}$ and $T_{\rm eS}$ is just 46 K.

4.3.10 KIC 5512589

We could not determine minima from its observed frequencies. We can only calculate $T_{\rm eVK}$ and $T_{\rm eBV}$ for this star. $T_{\rm eVK}$ is in good agreement with $T_{\rm eS}$.

4.3.11 KIC 5607242

KIC 5607242 is an evolved star. It shows mixed modes. Its $T_{\rm eS}$ is not available in the literature, therefore we use $T_{\rm eVK}$ in the scaling relations. $T_{\rm eBV}$ is about 500 K lower than $T_{\rm eVK}$. Furthermore, there is a systematic difference between photometric $T_{\rm eff}$s and asteroseismic $T_{\rm eff}$s. The observed value of $\nu_{\rm max}$ (610 μHz) gives $T_{\rm sis0}$ as 525 K higher than $T_{\rm eVK}$. If we take it as 652 μHz, the difference between $T_{\rm sis0}$ and $T_{\rm eVK}$ decreases to 345 K and optimum values are obtained for $M_{\rm sca}$ and $R_{\rm sca}$.

4.3.12 KIC 5689820

KIC 5689820 shows mixed modes. Observed oscillation frequencies do not allow determination of the frequencies of the minima. We compute its mass and radius from scaling relations, and photometric effective temperatures from colour.

4.3.13 KIC 5866724

The three-planet system KIC 5866724 is an F-like oscillating star (Chaplin et al. 2013). Conventional effective temperatures are very different and range from 5574 K to 6410 K. If we reduce $\nu_{\rm max}$ to 1844 μHz, $M_{\rm sca}$ is in very good agreement with $M_{\rm sis0}$ and $M_{\rm sis1}$. The same is true for the radii. The literature values are close to our results.

4.3.14 KIC 5955122

KIC 5955122 is an evolved star. The oscillation frequencies for $l = 1$ degree show mixed modes. KIC 5955122 is also a magnetically active star and has spots (Bonanno et al. 2014). It rotates faster than the Sun. There are two minima (min0 and min1) in its observed oscillation frequencies.

If we decrease $\nu_{\rm max}$ by an amount of 21 μHz, $T_{\rm eff}$s, masses, and radii computed from different methods are in good agreement but are larger than the values found in the literature.

4.3.15 KIC 6106415

The distance of KIC 6106415 is 41.48 pc. KIC 6106415 is one of the most well known stars in this study. Its asteroseismic $T_{\rm eff}$s with the observed value of $\nu_{\rm max}$ (2260 μHz) are in good agreement with non-asteroseismic $T_{\rm eff}$s. If we take $\nu_{\rm max}$ as 2188 μHz, then the agreement between asteroseismic $T_{\rm eff}$s and photometric $T_{\rm eff}$s is particularly excellent. The modified $\nu_{\rm max}$ also makes $M_{\rm sca}$ and $R_{\rm sca}$ equal to $M_{\rm sis0}$ and $R_{\rm sis0}$, respectively. Its $d_{\rm sis}$ determined from asteroseismic properties is 39.74 pc.

4.3.16 KIC 7106245

Its $T_{\rm eS}$ is not available in the literature. $T_{\rm eVK}$ is used in scaling relations. We have obtained $\nu_{\rm min1}$ from its observed oscillation frequencies. The observed value of $\nu_{\rm max}$ yields a $T_{\rm sis1}$ value 218 K higher than $T_{\rm eVK}$. If we increase $\nu_{\rm max}$ to 2375 μHz, the difference between $T_{\rm sis1}$ and $T_{\rm eVK}$ is 130 K. Meanwhile, $M_{\rm sca}$ and $R_{\rm sca}$ become very close to $M_{\rm sis1}$ and $R_{\rm sis1}$, respectively.

4.3.17 KIC 7341231

KIC 7341231 is a low-mass red giant and extremely metal-poor star ($[Fe/H] = -1.79$ dex). It may be a halo star (Sharma et al. 2016). Deheuvels et al. (2012) obtained the rotation rate of its core from observed oscillation frequencies. They inferred that the core of KIC 7341231 spins at least five times faster than its surface.

In this study, we obtain only $\nu_{\rm min0}$ from observed oscillation frequencies. If we decrease the observed $\nu_{\rm max}$ of KIC 7341231 from $\nu_{\rm max} = 408$ μHz to $\nu_{\rm max} = 387$ μHz, $T_{\rm sis0}$ becomes very close to $T_{\rm eS}$. However, there is a significant difference between $M_{\rm sis0}$ and $M_{\rm sca}$. A similar difference is also seen between $R_{\rm sis0}$ and $R_{\rm sca}$. Such differences may arise due to application of the relations derived from MS models to the red giants or very low metallicity of KIC 7341231.

4.3.18 KIC 7799349

KIC 7799349 is one of the coolest stars in our sample. It is a red giant star and with a spectral effective temperature of 4954 K. The $\Delta\nu$ versus ν diagram of KIC 7799349 has interesting features, including mixed modes. Despite the correction in $\nu_{\rm max}$, there are significant differences between the asteroseismic and non-asteroseismic effective temperature values. Also, there is no agreement for mass and radius values. The fitting formulae with $\nu_{\rm min1}$ may not be valid for such stars.

4.3.19 KIC 7871531

The $T_{\rm eS}$, $T_{\rm eVK}$ and $T_{\rm eBV}$ of KIC 7871531 are slightly different from each other. While $T_{\rm sis0}$ with $\nu_{\rm max} = 3344$ μHz is very close to $T_{\rm eS}$, $T_{\rm sis1}$ is 133 K greater than $T_{\rm eS}$. If $\nu_{\rm max}$ is taken as 3383 μHz, $T_{\rm sis0}$ is very close to $T_{\rm eVK}$ and $T_{\rm sis1}$ is nearly the same as $T_{\rm eS}$. The modified $\nu_{\rm max}$ (3383 μHz) makes $R_{\rm sca}$ equal to the other values for radius, 0.87. It also yields a $M_{\rm sca}$ in very good agreement with $M_{\rm sis0}$ and $M_{\rm sis1}$.

4.3.20 KIC 7976303

KIC 7976303 is a sub-giant star. Oscillation frequencies of KIC 7976303 shows mixed modes. Slightly modified $\nu_{\rm max}$ (856 μHz) makes $M_{\rm sca}$ equal to $M_{\rm sis0}$. $R_{\rm sca}$ from this $\nu_{\rm max}$ is very close to $R_{\rm lit}$, $R_{\rm sis0}$ and $R_{\rm sis1}$.

4.3.21 KIC 8219268

KIC 8219268 (Kepler-91) is a red giant and a planet host star. Kepler-91 b has been estimated to be a transiting Jupiter-mass planet (Lillo-Box et al. 2014). It is the coolest target star in this study, with a $T_{\rm eS}$ of 4550 K. If we slightly decrease the value of $\nu_{\rm max}$, we obtain better agreement between $T_{\rm eS}$ and $T_{\rm sis0}$ and between $R_{\rm sca}$ and $R_{\rm sis0}$. However, the difference between $M_{\rm sca}$ and $M_{\rm sis0}$ is high, as with other red giants.

4.3.22 KIC 8228742

Although the observed value of $\nu_{\rm max}$ (1171 μHz) gives $T_{\rm sis0}$ very close to $T_{\rm eS}$, $T_{\rm eVK}$ and $T_{\rm eBV}$, a slightly modified $\nu_{\rm max}$ (1139 μHz) yields $M_{\rm sca}$ exactly equal to $M_{\rm sis0}$ and $M_{\rm sis1}$.

4.3.23 KIC 8561221

KIC 8561221 is a red giant star. Oscillation frequencies of KIC 8561221 with degrees $l = 0$, 1, 2 and 3 are observed. If we modify $\nu_{\rm max}$, asteroseismic and non-asteroseismic effective temperatures are nearly the same, but there are significant differences between the asteroseismic and non-asteroseismic mass and radius values.

4.3.24 KIC 8694723

The asteroseismic and non-asteroseismic $T_{\rm eff}$s are in very good agreement. If we slightly modify $\nu_{\rm max}$, we obtain $M_{\rm sca}$ in perfect agreement with $M_{\rm sis0}$ and $M_{\rm sis1}$.

4.3.25 KIC 8760414

The $T_{\rm eS}$ of KIC 8760414 is the lowest temperature of five $T_{\rm eff}$s. If we take the value of $\nu_{\rm max}$ as 2333 μHz, $M_{\rm sca}$ becomes equal to 0.83 $M_\odot$, the same as $M_{\rm sis0}$ and $M_{\rm sis1}$.

4.3.26 KIC 9025370

The $T_{\rm eS}$ of this star is not available in the literature. Its $T_{\rm eVK}$ is used in the scaling relations. The observed value of $\nu_{\rm max}$ (2653 μHz) is so low that $T_{\rm sis0}$ is about 534 K higher than $T_{\rm eVK}$ (see Paper III). If the value of $\nu_{\rm max}$ is taken as 2977 μHz, all the asteroseismic masses and radii are equal to 1.00 $M_\odot$ and 1.01 $R_\odot$, respectively. This star seems to be a solar twin if its metallicity is similar to solar metallicity.

4.3.27 KIC 9139163

KIC 9139163 may be a component of KIC 9139151, another target star in the present study (Appourchaux et al. 2015). If this is true, these stars comprise a rare binary system in which the solar-like oscillating components are observed separately (White et al. 2016). Three minima are seen on the $\Delta\nu$ versus ν diagram of KIC 9139163. If we take $\nu_{\rm max}$ as 1672 μHz, all $T_{\rm eff}$s are in perfect agreement. This is also the case for the radii. For the mass, $M_{\rm sca}$ is very close to $M_{\rm sis0}$.

4.3.28 KIC 9206432

There are three minima on the $\Delta\nu$ versus ν diagram of KIC 9206432. $T_{\rm sis0}$, $T_{\rm sis1}$ and $T_{\rm sis2}$ are near to but less than the non-asteroseismic $T_{\rm eff}$s. The observed value of $\nu_{\rm max}$, 1853 μHz, yields masses and radii very different from each other. If we use 1759 μHz for $\nu_{\rm max}$, then $T_{\rm sis0}$, $T_{\rm sis1}$ and $T_{\rm sis2}$ are in much better agreement with non-asteroseismic $T_{\rm eff}$s. While $R_{\rm sca}$ is equal to $R_{\rm sis0}$, $M_{\rm sca}$ is very close to $M_{\rm sis1}$.

4.3.29 KIC 9410862

The $T_{\rm eS}$ of KIC 9410862 is not available in the literature. In scaling relations, we use $T_{\rm eVK}$. $\nu_{\rm min0}$ and $\nu_{\rm min1}$ are from oscillation frequencies with degree $l = 1$. Using the observed value of $\nu_{\rm max}$ (2261 μHz) causes a systematic difference between asteroseismic and non-asteroseismic $T_{\rm eff}$s. If we take $\nu_{\rm max}$ as 2235 μHz, the systematic differences decrease and excellent agreement is reached for the masses and radii. While $M_{\rm sca}$, $M_{\rm sis0}$ and $M_{\rm sis1}$ are all equal to 1.07 $M_\odot$, $R_{\rm sca}$, $R_{\rm sis0}$ and $R_{\rm sis1}$ all become equal to 1.20 $R_\odot$.

4.3.30 KIC 9812850

$T_{\rm sis1}$ and $T_{\rm sis2}$ are greater than the other $T_{\rm eff}$s. If we take the value of $\nu_{\rm max}$ as 1219 μHz, $T_{\rm sis1}$ becomes almost equal to $T_{\rm eBV}$, for example. With this modified value, $M_{\rm sca}$ is equal to $M_{\rm sis0}$ and $R_{\rm sca}$ is negligibly different from $R_{\rm sis0}$ and $R_{\rm sis1}$.

4.3.31 KIC 10162436

Three minima are seen on the $\Delta\nu$ versus ν diagram of KIC 10162436. All the asteroseismic $T_{\rm eff}$s with the observed $\nu_{\rm max}$ are higher than the non-asteroseismic $T_{\rm eff}$s. If $\nu_{\rm max}$ is taken as 1006 μHz, $T_{\rm sis0}$, $T_{\rm sis1}$ and $T_{\rm sis2}$ are all very close to $T_{\rm eBV}$, and $R_{\rm sca}$ is

very close to $R_{\rm sis0}$ and $R_{\rm sis1}$. $M_{\rm sca}$ with the modified $\nu_{\rm max}$ is very close to $M_{\rm sis1}$.

4.3.32 KIC 10454113

KIC 10454113 is among the stars for which we obtain amazing results. Its $\nu_{\rm max}$ is determined as 2261 μHz. $T_{\rm sis0}$ and $T_{\rm sis1}$ with this value are in good agreement with the non-asteroseismic $T_{\rm eff}$s. If we decrease $\nu_{\rm max}$to 2210 μHz, $M_{\rm sca}$ becomes the same as $M_{\rm sis0}$ and $M_{\rm sis1}$, 1.18 $M_{\odot}$. $R_{\rm sca}$ is in excellent agreement with $R_{\rm sis0}$ and $R_{\rm sis1}$.

4.3.33 KIC 11081729

KIC 11081729 is a very hot solar-like oscillating star. Although the observed value of $\nu_{\rm max}$ (1990 μHz) yields $T_{\rm sis0}$ and $T_{\rm sis1}$ in very good agreement with non-asteroseismic $T_{\rm eff}$s, we modify it (1977 μHz) to equalize $M_{\rm sca}$ to $M_{\rm sis1}$.

4.3.34 KIC 11244118

KIC 11244118 is a sub-giant star which is observed by *Kepler* with short cadence (58.85 s, Gilliland et al. 2013). Karoff et al. (2013) proposed that KIC 11244118 is an active star. Observed $\nu_{\rm max}$ is 1420 μHz. $T_{\rm sis0}$ is good agreement with $T_{\rm eS}$ and $T_{\rm eVK}$. $R_{\rm sis1}$ is equal to $R_{\rm sis0}$ and $M_{\rm sis1}$ and $M_{\rm sis0}$ are very close to each other.

4.3.35 KIC 11295426

KIC 11295426 (Kepler-68) is a planet host star. It has three planets (Gilliand et al. 2013). If $\nu_{\rm max}$ is taken as 2083 μHz, asteroseismic effective temperatures (except $T_{\rm sis1}$) are in excellent agreement with non-asteroseismic effective temperatures. Asteroseismic masses are in agreement with themselves and with the literature value.

4.3.36 KIC 11414712

KIC 11414712 is in sub-giant evolution stage with mixed modes. Its observed $\nu_{\rm max}$ is 707 μHz. Two minima are obtained from observed frequencies. $T_{\rm sis0}$ is slightly greater than non-asteroseismic $T_{\rm eff}$s but $M_{\rm sca}$ is very close to $M_{\rm sis0}$ and equal to $M_{\rm sis1}$.

4.3.37 KIC 11772920

Unfortunately, only $\nu_{\rm min0}$ is available from the $\Delta\nu$ versus ν diagram of KIC 11772920. Its observed $\nu_{\rm max}$ (3439 μHz) gives very high $T_{\rm sis0}$. The difference between $T_{\rm sis0}$ and $T_{\rm eS}$ is about 581 K. If $\nu_{\rm max}$ is taken as 3654 μHz, this difference is reduced to 192 K. Furthermore, $M_{\rm sca}$ with this value of $\nu_{\rm max}$ becomes very close to $M_{\rm sis0}$ and $R_{\rm sca}$ is equal to $R_{\rm sis0}$.

4.3.38 KIC 11807274

KIC 11807274 is an evolved star and hosts two planets (Chaplin et al. 2013). The observed value of $\nu_{\rm max}$ gives $T_{\rm sis1}$ in very good agreement with $T_{\rm eS}$. However, $T_{\rm sis0}$ is 282 K is higher than $T_{\rm eS}$. In order to obtain agreement between $R_{\rm sca}$, $R_{\rm sis0}$ and $R_{\rm sis1}$, $\nu_{\rm max}$ is decreased to 1472 μHz. With this value of $\nu_{\rm max}$, $M_{\rm sca}$ is equal to $M_{\rm sis1}$.

4.3.39 KIC 12069424

One of the brightest $Kepler$ targets is KIC 12069424 (16 Cyg A), an evolved star. Metcalfe et al. (2012) identify 46 oscillation frequencies, including the modes with $l = 3$. They determine the fundamental properties of this star by constructing interior models with different stellar evolution codes. If we slightly increase (42 μHz) the value of $\nu_{\rm max}$, $R_{\rm sca}$ becomes equal to $R_{\rm sis0}$ and $R_{\rm sis1}$. With the modified $\nu_{\rm max}$, $M_{\rm sca}$ is very close to $M_{\rm sis0}$ and $M_{\rm sis1}$. The asteroseismic distance of KIC 12069424 is almost the same as the observed distance.

4.3.40 KIC 12069449

KIC 12069449 (16 Cyg B) is an MS star and hosts a planet. Its observed $\nu_{\rm max}$ is 2552 μHz. This value yields a $T_{\rm sis0}$ lower than the non-asteroseismic $T_{\rm eff}$s and a $T_{\rm sis1}$ slightly higher than them. If we take $\nu_{\rm max}$ as 2485 μHz, $T_{\rm sis0}$ is very close to $T_{\rm eBV}$ and $M_{\rm sca}$ is equal to $M_{\rm sis0}$. With the modified $\nu_{\rm max}$, the asteroseismic radii are in very good agreement.

4.3.41 HD 2151

HD 2151 (β Hyi, HR 98, HIP 2021) is a bright sub-giant star. Bedding et al. (2007) have observed frequencies of this star using high-precision velocity observation with HARPS and UCLES spectrographs. They also identified 28 modes with degrees $l = 0$, 1 and 2. $M_{\rm sca}$ is in very good agreement with $M_{\rm sis0}$ and $M_{\rm sis1}$. This star is very close at a distance of 7.46 pc (from Hipparcos parallax). We determined its asteroseismic distance to be 7.08 pc, very similar to the observed value.

4.3.42 HD 43587

The evolved star HD 43587 shows mixed modes in its oscillation frequencies, which were observed by *CoRoT* (Boumier et al. 2014). If we decrease observed $\nu_{\rm max}$ to 2228 μHz, asteroseismic and non-asteroseismic $T_{\rm eff}$s (except $T_{\rm sis1}$) are in very good agreement. The asteroseismic radii of HD 43587 are in excellent agreement and $M_{\rm sca}$ is very close to $M_{\rm sis0}$ and $M_{\rm sis1}$.

4.3.43 HD 146233

Target star HD 146233 (18 Sco) was identified as a solar twin (Porto de Mello & de Silva 1997). The oscillation frequencies of this star are obtained by HARPS spectrometer. $T_{\rm eff}$s are very different from each other, but $T_{\rm eS}$ is very close to $T_{\rm eBV}$. If we take $\nu_{\rm max}$ as 3000 μHz, $T_{\rm sis1}$ is in good agreement with $T_{\rm eVK}$. This value of $\nu_{\rm max}$ yields a $M_{\rm sca}$ in better agreement with $M_{\rm sis0}$ and $M_{\rm sis1}$. All the asteroseismic radii are in excellent agreement with the interferometric radius obtained by Bazot et al. (2011) as 1.010$\pm$ 0.009 $R_{\odot}$.

4.3.44 Procyon A

Procyon is a spectroscopic binary system and Procyon A shows solar-like oscillations. The oscillation frequencies of Procyon A are obtained through a multi-site spectroscopic campaign (Bedding et al. 2010). It is the closest star (3.51 pc, from Hipparcos parallax) in our sample. Its mass and radius are determined with non-asteroseismic methods using *Hubble Space Telescope* and ground-based astrometric data.

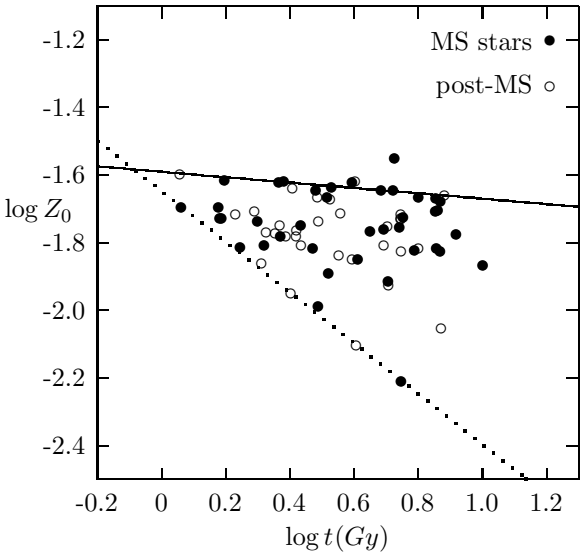

Figure 8. $\log Z_0$ is plotted with respect to logarithm of age. The filled circles are for MS and the circles are for post-MS stars. The solid line represents time variation of maximum metallicity ($-0.08 \log t - 1.59$). The dotted line shows time variation of minimum metallicity ($-0.75 \log t - 1.65$). It is very interesting that the relation between the logarithm of the lowest metallicity and $\log t$ is well represented by a linear equation: $Z_{0\rm min} \propto t^{-0.75}$

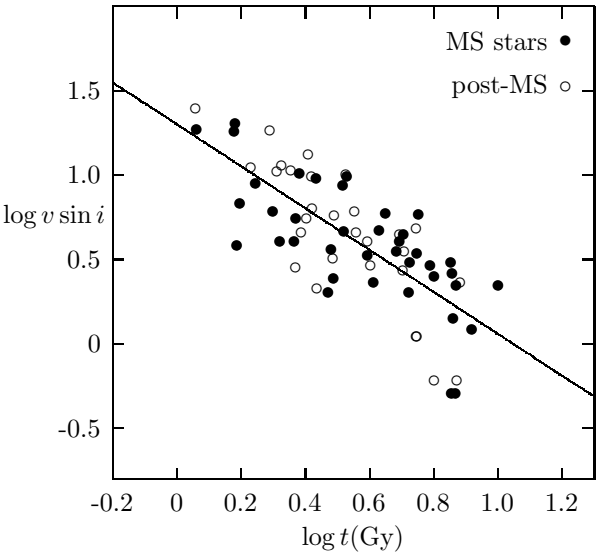

Figure 9. $\log v \sin i$ is plotted with respect to logarithm of age. The filled circles are for MS and the circles are for post-MS stars. These stars obey the same law despite being in different evolutionary phases. The solid line shows mean time variation of $\log v \sin i$: $\log v \sin i = -1.24 \log t + 1.3$.

The observed mass of sub-giant Procyon A is 1.478 $\pm$ 0.012 $M_\odot$ (Bond et al. 2015). The interferometric radius of Procyon A is 2.031 $\pm$ 0.013 $R_\odot$ (Aufdenberg, Ludwig & Kervella 2005). In this study, the observed $\nu_{\rm max}$ of Procyon A is increased by only 5 μHz. When we use the modified $\nu_{\rm max}$ in scaling relations, asteroseismic mass and radius are in excellent agreement with non-asteroseismic values. Also, asteroseismic effective temperatures are compatible with $T_{\rm eS}$.

5 CONSEQUENCES OF THE FINDINGS

5.1 Chemical evolution of the galactic disc

Metallicity is very important for our understanding of stellar evolution in two respects. Firstly, it dramatically influences the inner core as much as the outer regions. Secondly, it in turn implicitly represents stellar age because heavy element abundances in the galactic disc increase in time. However, to date, the relation between heavy metal abundances and time has not been fully elucidated.

In Fig. 8, $\log Z_0$ is plotted against $\log(t)$ and yields very striking results. There is a continuous metal enrichment in all stages for both MS and post-MS stars. Different ages have different metallicity intervals. There are very old stars with high metallicity. For example, some of the stars with ages of about 7 Gyr have Z_0 ($\log Z_0 = -1.6$) of about 0.022. The maximum metallicity of the youngest stars (about 0.025) is slightly higher than this value. This implies that the maximum metallicity does not change very rapidly over time, at least during the last 7 Gyr. However, for all ages, there is a minimum metallicity and it changes so rapidly that there is no young star with low-metallicity in our sample. These confirmations may be very important for our understanding of the chemical evolution of the Galaxy as a result of repeatedly reprocessing stellar material.

5.2 Gyrochronology

The magnetic braking mechanism is responsible for the slow rotation of late-type stars with convective envelope. For most of the target stars, rotational velocity ($v \sin i$) is available in the literature. The $v \sin i$ values are taken from Pinsonneault et al. (2014). Their logarithmic values are plotted with respect to $\log t$ in Fig. 9. There is a very clear inverse relation between $\log(v \sin i)$ and $\log t$. Furthermore, the MS and the post-MS stars obey the same relation. The slope of this line is -1.24. This means that rotational velocity is inversely proportional to $t^{5/4}$ for all mass intervals for solar-like oscillating stars. The power of t is $1/2$ in the original Skumanich relation (Skumanich 1972).

6 CONCLUSIONS

The He II ionization zone causes $\Delta\nu$ to have an oscillatory component in the spacing of oscillation frequencies. Both models and observations have several minima in the $\Delta\nu$ versus ν graph. In our previous papers, we have already shown that the frequencies of these minima have very strong diagnostic potential for determination of the fundamental properties of solar-like oscillating stars. The $T_{\rm eff}$s of about 90 stars were obtained from their oscillation frequencies in Paper III. In the present study, we develop new methods for determining M, R, g and age using models constructed with the MESA code and apply the methods to these stars.

The precision of new relations for M and R are comparable to the new scaling relations with Γ_{1s} presented in Paper III. However, uncertainties in $M_{\rm sca}$ and $R_{\rm sca}$ are not low enough for many stars because $\nu_{\rm max}$ cannot be obtained very accurately for many of the solar-like oscillating stars. Therefore, $M_{\rm sis0}$ and $M_{\rm sis1}$ are much more accurate than $M_{\rm sca}$. The mass and radius range of the targets are determined to be [0.8,1.8] $M_\odot$ and [0.85,13] $R_\odot$, respectively. The maximum difference between $M_{\rm sis1}$ and $M_{\rm sis0}$ is about 4 per cent and very precise results are obtained for 34 of these stars: $\mid M_{\rm sis0} - M_{\rm sis1} \mid < 0.02$ $M_\odot$ and $\mid R_{\rm sis0} - R_{\rm sis1} \mid < 0.007$ $R_\odot$.

This shows that frequencies $\nu_{\rm min0}$, $\nu_{\rm min1}$ and $\nu_{\rm min2}$ have strong diagnostic potentials for the determination of fundamental properties of stars, including mass and radius.

We also compute the age and initial metallicity of the target stars and obtain very interesting results regarding the relation between age and metallicity (see Fig 8). It seems that every time has its own Z interval in the galactic disc and there is a very clear relation in particular between the minimum Z and age.

Once we obtain $M_{\rm sis0}$ and $R_{\rm sis0}$, we modify the value of $\nu_{\rm max}$ so that all three quantities $T_{\rm eff}$, $M_{\rm sca}$ and $R_{\rm sca}$ are in better agreement with $T_{\rm sis0}$, $M_{\rm sis0}$ and $R_{\rm sis0}$. The same is true for $M_{\rm sis1}$ and $R_{\rm sis1}$, of course. In that way, we can precisely determine the value of $\nu_{\rm max}$.

We also obtain an inverse relation between age and $v\sin(i)$: $v\sin(i) \propto t^{-1.24}$. This relation is significantly different from the Skumanich relation, in which $v\sin(i) \propto t^{-0.5}$.

ACKNOWLEDGEMENTS

We would like to thank Jacqueline Renee Gutenkunst for her help in checking the language of the manuscript. This work is supported by the Scientific and Technological Research Council of Turkey (TÜBİTAK: 112T989).

REFERENCES

Appourchaux T. et al., 2015, A&A, 582, A25
Arentoft T. et al., 2008, ApJ, 687, 1180
Aufdenberg J. P., Ludwing H. G., Kervella P., 2005, ApJ, 633, 424
Bahcall J. N., Serenelli A. M., Pinsonneault M., 2004, ApJ, 614, 464
Ballard S. et al., 2014, ApJ, 790, 12
Bazot M. et al., 2011, A&A, 526, L4
Bedding T. R. et al., 2007, ApJ, 663, 1315
Bedding T. R. et al., 2010, ApJ, 713, 935
Benomar O., Masuda K., Shibahashi H., Suto Y., 2014, PASJ, 66, 94
Bond H. et al, 2015, ApJ, 813, 2
Bonanno A., Frohlich H. E., Karoff C., Lund M. N., Corsaro E. Frasca A., 2014, A&A, 569, A113
Boumier P. et al., 2014, A&A, 564, A34
Bruntt H. et al., 2012, MNRAS, 423, 122
Chaplin W. J. et al., 2013, ApJ, 766, 101
Deheuvels S. et al., 2012, ApJ, 756, 19
Edvardsson B., Andersen J., Gustafsson B., Lambert D. L., Nissen P. E., Tomkin J., 1993, A&A, 275, 101
Gaia Collaboration, Prusti T., de Bruijne J. H. J., et al. 2016, A&A, doi:10.1051/0004-6361/201629272
Gilliland R. L. et al., 2013, ApJ, 766, 40
Gruyters P., Nordlander T., Korn A. J., 2014, A&A, 567, A72
Gruyters P. et al., 2016, A&A, 589, A61
Howell R. L. et al., 2012, ApJ, 746, 123
Huber D. et al., 2011, ApJ, 743, 143
Kallinger T. et al., 2010, A&A, 522, A1
Karoff C. et al., 2013, MNRAS, 433, 3227
King J. R., Stephens A., Boesgaard A. M., Deliyannis C., 1998, ApJ, 115, 666
Korn A. J., Grundahl F., Richard O., Mashonkina L., Barklem P. S., Collet R., Gustafsson B., Piskunov N., 2007, ApJ, 671, 402
Lillo-Box J. et al., 2014, A&A, 562, A109
Mathur S. et al., 2012, ApJ, 749, 152
Metcalfe T. S. et al., 2012, ApJ, 748, L10
Michaud G., Proffitt C. R., 1993, in Weiss W. W., Baglin A., eds, Astronomical Society of the Pacific Conference Series Vol. 40, IAU Colloq. 137: Inside the Stars. pp 246-259
Molenda-Żakowicz J. et al., 2013, MNRAS, 434, 1422
Neilsen M. B., Schunker H., Gizon L., Ball W. H., 2015, A&A, 582, A10
Paxton, B., Bildsten, L., Dotter, A., Herwig, F., Lesaffre, P., Timmes, F., 2011, ApJS, 192, 3
Perryman M. A. C. Lindegren L., Kovalevsky J., et al. 1997, A&A, 323, 49
Pinsonneault M. H. et al., 2014, ApJS, 215, 19
Porto de Mello G. F. & da Silva L., 1997, ApJ, 482, 289
Sharma S., Stello D., Bland-Hawthorm J., Huber D., Bedding T. R., 2016, ApJ, 822, 15
Stello D., Bruntt H., Preston H., Buzasi D., 2008, ApJ, 674, L53
Skumanich A., 1972, ApJ, 171, 565
Thoul A. A., Bahcall J. N., Loeb A., 1994, ApJ, 421, 828
White T. R. et al., 2016, A&A, in press
Yıldız M., 2011, MNRAS, 412, 2571
Yıldız M., Çelik Orhan Z., Aksoy C., Ok S., 2014a, MNRAS, 441, 2148 (Paper I)
Yıldız M., Çelik Orhan Z., Kayhan C., Turkoglu G. E., 2014b, MNRAS, 445, 4395
Yıldız M., Çelik Orhan Z., Kayhan C., 2015, MNRAS, 448, 3689 (Paper II)
Yıldız M., Çelik Orhan Z., Kayhan C., 2016, MNRAS, 462, 1577 (Paper III)
Yıldız M., Çelik Orhan Z., Örtel S., Roth M., 2017, submitted to MNRAS

APPENDIX A: BASIC ASTEROSEISMIC AND NON-ASTEROSEISMIC PROPERTIES OF *KEPLER* AND *COROT* TARGETS

Table A1: Basic properties of *Kepler* and *CoRoT* targets. Columns are organized as star name, frequency of maximum amplitude, reference frequencies for min0, min1 and min2, mean large and small separations between oscillation frequencies, effective temperatures (from spectra, V-K and B-V colours (see section 2 in Paper III) and from minima min0, min1 and min2 (see section 3 in Paper III), respectively), masses and radii (from new scaling relation (see section 3 in Paper III), from min0 and min1 and from literature, respectively), distances (from literature and from seismic), surface gravities (from new scaling relations (see section 3 in Paper III), from seismic (see Section 2.) and from spectra, respectively), ages (from seismic (see Section 2.) and from method that based on mass, radius and metallicity (see Yıldız et al. 2014b for details), metallicities (from spectra and from computed with diffusion (see Section 3.)) and numbers of references. Second row describes uncertainities of basic properties. Unlike others, for Procyon A, mass and radius are the observed values, not the model values in the literature. Sun is denoted by ⊙ symbol at the end of the table.

Star	$\nu_{\rm max}$	$\nu_{\rm min0}$	$\nu_{\rm min1}$	$\nu_{\rm min2}$	$\Delta\nu$	$\langle\delta\nu_{02}\rangle$	$T_{\rm eS}$	$T_{\rm eVK}$	$T_{\rm eBV}$	$T_{\rm sis0}$	$T_{\rm sis1}$	$T_{\rm sis2}$	$M_{\rm sca}$	$M_{\rm sis0}$	$M_{\rm sis1}$	$M_{\rm lit}$	$R_{\rm sca}$	$R_{\rm sis0}$	$R_{\rm sis1}$	$R_{\rm lit}$	$d_{\rm obs}$	$d_{\rm sis}$	$g_{\rm sca}$	$g_{\rm sis}$	$g_{\rm spc}$	$t_{\rm sis}$	$t_{\rm yil}$	$Z_{\rm s}$	Z_0	Ref
	μHz	μHz	μHz	μHz	μHz	μHz	K	K	K	K	K	K	$M_\odot$	$M_\odot$	$M_\odot$	$M_\odot$	$R_\odot$	$R_\odot$	$R_\odot$	$R_\odot$	pc	pc				Gyr	Gyr			
1435467	1364.0	1626.4	1274.0	—	70.9	4.8	6264	6224	6587	6149	6326	—	1.29	1.26	1.29	1.27	1.66	1.66	1.67	1.64	178.65	133.86	4.11	4.10	4.09	3.36	3.36	0.0133	0.0212	2,13,17
	40.9	16.3	12.7	—	0.8	—	60	51	185	100	104	—	0.19	0.02	0.02	0.05	0.10	0.01	0.01	0.03	0.04	1.23	0.01	0.01	0.03	0.25	—	0.0006	0.0006	39
2837475	1550.0	2265.6	1689.9	1276.8	75.2	6.7	6462	6545	6488	6485	6592	6661	1.51	1.57	1.52	1.39	1.67	1.67	1.66	1.59	126.02	115.87	4.17	4.18	3.95	1.15	0.96	0.0125	0.0200	2,17,39
	54.0	22.7	16.9	12.8	1.3	—	125	54	144	14	52	75	0.31	0.03	0.03	0.06	0.13	0.02	0.02	0.03	0.03	5.87	0.02	0.02	0.23	0.11	0.11	0.0017	0.0018	40
3424541	731.0	1046.6	755.4	—	41.1	4.7	6165	6249	6322	6443	6519	—	1.74	1.81	1.75	1.64	2.65	2.66	2.64	2.53	305.86	307.62	3.83	3.84	3.90	1.14	2.20	0.0156	0.0250	2,17,39
	55.0	10.5	7.6	—	1.1	—	108	73	249	49	124	—	0.63	0.04	0.04	0.04	0.36	0.03	0.03	0.07	0.07	10.55	0.02	0.02	0.21	0.16	0.56	0.0020	0.0023	40
3427720	2638.0	3044.3	2325.2	—	120.0	10.3	6040	6038	6055	6104	6091	—	1.11	1.13	1.11	1.13	1.12	1.12	1.12	1.13	95.11	92.52	4.38	4.39	4.38	2.09	2.30	0.0129	0.0155	2,13,17
	191.0	30.4	23.3	—	2.0	—	60	60	211	253	345	—	0.33	0.03	0.03	0.04	0.12	0.02	0.02	0.01	0.02	25.24	0.02	0.02	0.03	0.19	0.21	0.0006	0.0012	39
3544595	3226.0	3350.9	2702.9	—	145.5	8.7	5689	5640	5434	5561	5843	—	0.89	0.89	0.92	0.91	0.92	0.92	0.92	0.92	98.70	94.19	4.46	4.47	4.56	7.39	4.25	0.0112	0.0149	4,29,46
	81.0	33.5	27.0	—	1.5	—	48	52	200	219	181	—	0.11	0.02	0.02	0.06	0.05	0.01	0.01	0.02	0.03	10.52	0.01	0.01	0.06	0.49	0.63	0.0008	0.0020	
3632418	1100.0	1370.9	1055.0	—	60.4	3.8	6148	6154	6148	6241	6394	—	1.27	1.27	1.29	1.27	1.85	1.84	1.85	1.83	110.66	101.79	4.01	4.01	3.94	2.64	2.64	0.0107	0.0171	2,17,39
	44.0	13.7	10.6	—	0.4	—	111	38	77	93	108	—	0.22	0.02	0.02	0.03	0.12	0.01	0.01	0.03	0.02	1.99	0.01	0.01	0.21	0.14	0.63	0.0015	0.0015	40
3656476	1887.0	—	—	—	93.2	4.4	5710	5752	5303	—	—	—	1.06	—	—	1.09	1.31	—	—	1.32	115.84	110.91	4.23	—	4.23	—	8.16	0.0198	0.0228	13,17,37
	40.0	—	—	—	1.3	—	60	52	137	—	—	—	0.14	—	—	0.01	0.07	—	—	0.03	0.03	—	0.01	—	0.03	—	0.63	0.0010	0.0010	
3733735	2001.0	—	2211.0	1480.0	91.6	9.9	6548	6610	6581	—	6610	6462	1.48	—	1.49	1.32	1.45	—	1.45	1.37	104.29	97.50	4.28	4.29	3.99	0.05	—	0.0116	0.0186	2,17,39
	121.0	—	22.1	14.8	2.5	—	156	43	151	—	75	220	0.48	—	0.04	0.04	0.18	—	0.03	0.02	0.03	—	0.02	0.02	0.22	0.01	—	0.0016	0.0070	40
3735871	2633.0	2850.7	—	—	124.7	12.3	5908	6207	5908	5797	—	—	0.93	1.04	—	1.07	1.03	1.08	—	1.09	126.54	103.53	4.38	—	—	—	—	—	—	2,17
	79.0	28.5	—	—	3.3	—	100	49	202	189	—	—	0.21	0.04	—	0.12	0.09	0.03	—	0.05	0.03	15.96	0.02	—	—	—	—	—	—	
4349452	2060.0	2568.7	1884.4	—	97.6	7.7	6270	6194	6048	6309	6245	—	1.24	1.27	1.21	1.19	1.33	1.33	1.32	1.31	254.26	244.64	4.29	4.28	4.28	2.71	3.22	0.0128	0.0177	9,29,36
	50.0	25.7	18.8	—	1.0	—	79	107	—	59	111	—	0.16	0.02	0.02	0.06	0.07	0.01	0.01	0.02	0.07	9.72	0.01	0.01	0.03	0.18	0.68	—	0.0006	
4914923	1775.0	1947.8	—	—	88.7	6.1	5808	5721	5910	5843	—	—	1.10	1.10	—	1.10	1.37	1.38	—	1.37	137.47	117.79	4.20	—	4.28	—	6.13	0.0156	0.0217	17,37,40
	46.0	19.5	—	—	0.3	—	92	65	194	153	—	—	0.13	0.01	—	0.01	0.06	—	—	0.05	0.04	4.50	0.01	—	0.21	—	0.68	0.0020	0.0020	
5184732	1978.0	2182.6	1705.5	—	95.1	5.9	5840	5836	5611	5886	6033	—	1.15	1.15	1.17	1.25	1.33	1.33	1.33	1.36	70.46	67.14	4.25	4.25	4.26	5.83	7.51	0.0208	0.0280	13,17,37
	47.0	21.8	17.1	—	1.3	—	60	41	91	142	138	—	0.16	0.03	0.03	0.01	0.07	0.01	0.01	0.01	0.02	2.43	0.01	0.01	0.03	0.49	0.68	0.0010	0.0010	
5512589	1224.0	—	—	—	68.2	5.5	5764	5687	5583	—	—	—	1.02	—	—	1.16	1.60	—	—	1.67	204.20	181.48	4.04	—	4.22	—	7.83	0.0144	0.0224	17,37,40
	43.0	—	—	—	0.7	—	95	64	203	—	—	—	0.17	—	—	0.01	0.10	—	—	0.01	0.05	—	0.01	—	0.21	—	0.68	0.0019	0.0019	
5607242	652.0	745.3	543.4	—	40.5	3.7	5572	5572	5070	5917	6075	—	1.18	1.15	1.14	1.33	2.37	2.39	2.38	2.49	369.84	322.82	3.76	3.74	—	—	—	—	—	2,17
	19.6	7.5	5.4	—	0.8	—	100	83	272	125	121	—	0.23	0.03	0.03	0.11	0.19	0.02	0.02	0.10	0.10	5.93	0.02	0.02	—	—	—	—	—	
5689820	695.0	—	—	—	41.0	3.9	4978	—	—	—	—	—	1.11	—	—	1.14	2.29	—	—	—	345.71	314.29	3.76	—	—	—	6.30	0.0177	0.0167	22
	15.0	—	—	—	0.5	—	167	—	—	—	—	—	0.18	—	—	—	0.14	—	—	—	0.09	—	0.01	—	—	—	—	0.0011	0.0011	
5866724	1844.0	2171.6	1674.4	—	89.6	6.6	6211	6410	5574	6142	6229	—	1.25	1.25	1.25	1.27	1.41	1.42	1.42	1.42	282.90	273.06	4.24	4.23	4.23	3.38	5.07	0.0164	0.0230	16,29
	60.0	21.7	16.7	—	0.9	—	167	104	369	115	138	—	0.22	0.02	0.02	0.06	0.09	0.01	0.01	0.02	0.10	18.41	0.01	0.01	0.01	0.23	1.14	0.0008	0.0022	
5955122	840.0	952.7	717.9	—	49.4	4.8	5952	5917	6068	5913	6120	—	1.24	1.22	1.24	1.12	2.10	2.14	2.14	2.04	191.80	180.51	3.88	3.87	4.13	3.61	3.61	0.0126	0.0192	2,17,39

Table A1: – continued from previous page

Star	$\nu_{\rm max}$	$\nu_{\rm min0}$	$\nu_{\rm min1}$	$\nu_{\rm min2}$	$\Delta\nu$	$\langle\delta\nu_{02}\rangle$	$T_{\rm eS}$	$T_{\rm eVK}$	$T_{\rm eBV}$	$T_{\rm sis0}$	$T_{\rm sis1}$	$T_{\rm sis2}$	$M_{\rm sca}$	$M_{\rm sis0}$	$M_{\rm sis1}$	$M_{\rm lit}$	$R_{\rm sca}$	$R_{\rm sis0}$	$R_{\rm sis1}$	$R_{\rm lit}$	$d_{\rm obs}$	$d_{\rm sis}$	$g_{\rm sca}$	$g_{\rm sis}$	$g_{\rm spc}$	$t_{\rm sis}$	$t_{\rm yil}$	$Z_{\rm s}$	Z_0	Ref
	μHz	μHz	μHz	μHz	μHz	μHz	K	K	K	K	K	K	$M_\odot$	$M_\odot$	$M_\odot$	$M_\odot$	$R_\odot$	$R_\odot$	$R_\odot$	$R_\odot$	pc	pc				Gyr	Gyr			
	24.0	9.5	7.2	—	0.9	—	100	78	192	128	118	—	0.23	0.03	0.03	0.05	0.15	0.02	0.02	0.03	0.05	6.08	0.02	0.02	0.21	0.37	1.14	0.0019	0.0019	40
6106415	2188.0	2533.1	1909.2	—	103.9	6.5	5990	6056	6040	6095	6074	—	1.13	1.13	1.10	1.12	1.24	1.23	1.23	1.24	41.48	39.74	4.30	4.30	4.31	4.94	5.23	0.0121	0.0172	13,17,37
	53.0	25.3	19.1	—	0.3	—	60	50	76	105	136	—	0.11	0.01	0.01	0.02	0.04	—	—	0.01	0.01	4.46	0.01	0.01	0.03	0.19	1.07	0.0006	0.0006	
6116048	2028.0	2250.4	1748.1	—	100.5	5.9	5991	6109	5844	5900	6051	—	1.03	1.03	1.03	1.12	1.23	1.23	1.23	1.26	75.15	70.21	4.27	4.27	4.09	6.15	6.00	0.0101	0.0150	2,3,37
	60.8	22.5	17.5	—	0.2	—	124	41	119	160	157	—	0.13	0.01	0.01	0.02	0.06	—	—	0.01	0.02	2.10	0.01	0.01	0.22	0.23	0.92	0.0017	0.0020	40
6508366	926.0	1267.5	978.3	672.2	51.5	3.3	6354	6268	6414	6400	6548	6551	1.46	1.45	1.48	1.36	2.14	2.12	2.13	2.08	188.48	182.23	3.94	3.95	3.94	1.95	2.51	0.0122	0.0195	2,13,17
	36.0	12.7	9.8	6.7	0.8	—	60	60	177	43	64	101	0.28	0.03	0.03	0.04	0.16	0.02	0.02	0.02	0.05	2.95	0.01	0.01	0.03	0.18	0.66	0.0006	0.0064	39
6603624	2402.0	2529.7	2080.5	—	109.7	5.5	5625	5642	5364	5649	6017	—	1.12	1.00	1.05	1.09	1.20	1.15	1.16	1.18	83.56	82.65	4.33	4.33	4.32	7.13	7.84	0.0175	0.0235	2,13,17
	51.0	25.3	20.8	—	1.7	—	60	58	113	179	137	—	0.16	0.03	0.03	0.03	0.07	0.02	0.02	0.02	0.02	9.52	0.01	0.01	0.03	0.65	0.43	0.0009	0.0056	39
6679371	916.0	1284.8	1000.6	725.8	50.6	4.1	6344	6375	6453	6429	6584	6652	1.52	1.53	1.58	1.56	2.19	2.18	2.19	2.19	179.09	163.44	3.94	3.95	3.92	1.70	1.86	0.0119	0.0171	2,3,39
	27.5	12.8	10.0	7.3	0.7	—	131	21	132	28	43	60	0.27	0.03	0.03	0.03	0.15	0.01	0.01	0.02	0.04	4.29	0.01	0.01	0.21	0.14	0.53	0.0016	0.0054	40
6933899	1366.0	1538.7	1178.0	—	71.8	4.9	5837	5700	5982	5938	6089	—	1.17	1.16	1.17	1.14	1.61	1.61	1.62	1.60	141.88	157.07	4.09	4.09	4.21	5.27	5.27	0.0141	0.0225	2,17,39
	32.0	15.4	11.8	—	1.0	—	97	58	191	120	118	—	0.18	0.03	0.03	0.03	0.10	0.01	0.01	0.02	0.05	12.35	0.01	0.01	0.22	0.44	0.53	0.0019	0.0029	40
7103006	1124.0	1432.9	1134.4	790.3	60.1	4.5	6394	6351	6151	6302	6486	6480	1.41	1.38	1.43	1.43	1.90	1.90	1.92	1.90	161.90	152.93	4.03	4.03	4.01	2.56	3.28	0.0142	0.0228	2,13,17
	54.0	14.3	11.3	7.9	1.1	—	60	42	126	89	100	147	0.33	0.03	0.03	0.05	0.17	0.02	0.02	0.03	0.04	6.80	0.02	0.02	0.03	0.26	0.76	0.0007	0.0043	39
7106245	2375.0	—	2105.0	—	111.6	7.0	6000	6000	5725	—	6130	—	1.08	—	1.09	—	1.17	—	1.16	—	—	200.20	4.34	4.34	—	—	—	—	—	2
	71.2	—	21.0	—	1.1	—	99	98	479	—	152	—	0.17	—	0.02	—	0.07	—	0.01	—	—	—	0.01	0.01	—	—	—	—	—	
7206837	1602.0	2023.7	1545.1	1153.7	78.7	6.2	6304	6190	6480	6320	6396	6461	1.38	1.39	1.38	1.46	1.59	1.59	1.58	1.56	207.98	194.52	4.18	4.18	4.17	2.41	3.56	0.0158	0.0240	2,13,17
	70.0	20.2	15.5	11.5	1.4	—	60	60	263	83	129	154	0.30	0.03	0.03	0.05	0.13	0.02	0.02	0.02	0.08	5.39	0.02	0.02	0.03	0.24	1.06	0.0008	0.0017	39
7341231	387.0	384.5	—	—	28.8	3.4	5233	5440	5438	5243	—	—	0.88	0.71	—	0.90	2.69	2.62	—	2.69	248.71	218.29	3.52	—	3.54	—	5.57	0.0028	0.0026	2,17,21
	8.0	3.8	—	—	0.7	—	50	51	180	146	—	—	0.15	0.04	—	0.10	0.20	0.02	—	0.20	0.05	7.41	0.02	—	0.03	—	1.06	0.0001	0.0001	
7680114	1684.0	—	—	—	85.1	—	5799	5891	5588	—	—	—	1.10	—	—	1.19	1.41	—	—	1.45	169.48	163.01	4.18	—	4.25	—	5.78	0.0147	0.0218	17,37,40
	47.0	—	—	—	1.3	—	91	94	268	—	—	—	0.19	—	—	0.01	0.09	—	—	0.03	0.05	—	0.01	—	0.21	—	1.06	0.0019	0.0019	
7747078	917.0	1039.3	792.5	—	53.4	4.7	5840	5754	5727	5915	6148	—	1.16	1.13	1.15	1.06	1.96	1.96	1.97	1.89	183.66	171.12	3.92	3.91	3.91	3.57	3.57	0.0098	0.0145	2,13,17
	32.0	10.4	7.9	—	0.3	—	60	66	172	150	135	—	0.17	0.02	0.02	0.05	0.10	0.01	0.01	0.02	0.04	6.36	0.01	0.01	0.03	0.18	1.06	0.0004	0.0004	39
7799349	561.0	580.6	448.6	—	33.2	3.4	4954	4962	4821	5479	5902	—	1.34	1.05	1.10	1.39	2.80	2.65	2.68	—	187.59	174.37	3.67	3.62	3.33	5.58	5.58	0.0158	0.0149	2,22,40
	8.0	5.8	4.5	—	0.4	—	92	41	124	124	87	—	0.16	0.02	0.02	—	0.13	0.01	0.01	—	0.04	4.48	0.01	0.01	0.22	0.43	1.06	0.0020	0.0020	
7871531	3383.0	3403.0	2658.3	—	151.3	10.1	5400	5289	5641	5324	5432	—	0.81	0.82	0.81	0.84	0.87	0.87	0.87	0.87	65.73	60.31	4.47	4.47	4.49	10.03	6.78	0.0101	0.0135	2,13,39
	101.5	34.0	26.6	—	3.6	—	60	51	145	301	270	—	0.16	0.04	0.04	0.02	0.07	0.02	0.02	0.01	0.06	8.02	0.02	0.02	0.20	1.20	0.75	0.0014	0.0020	
7976303	856.0	1036.3	754.0	—	51.0	4.5	6053	5967	6315	6125	6210	—	1.17	1.17	1.14	1.17	2.01	2.03	2.02	2.03	156.36	161.94	3.90	3.88	3.87	2.53	2.53	0.0070	0.0111	13,17,37
	20.0	10.4	7.5	—	0.6	—	60	66	182	78	89	—	0.15	0.02	0.02	0.02	0.10	0.01	0.01	0.05	0.04	4.17	0.01	0.01	0.03	0.18	0.37	0.0003	0.0003	
8006161	3481.0	3518.3	2922.7	—	149.2	10.3	5390	5378	5189	5365	5800	—	0.93	0.92	0.96	1.00	0.92	0.92	0.92	0.93	27.17	26.28	4.48	4.49	4.49	6.32	6.24	0.0175	0.0214	2,13,17
	133.0	35.2	29.2	—	1.8	—	60	—	—	367	275	—	0.17	0.02	0.02	0.01	0.06	0.01	0.01	—	0.01	2.83	0.01	0.01	0.03	0.49	0.96	0.0009	0.0014	37
8026226	545.0	687.7	479.1	—	34.6	3.6	6230	6233	6204	6202	6227	—	1.45	1.42	1.35	1.50	2.80	2.82	2.80	2.75	192.94	176.24	3.71	3.67	3.71	2.26	2.26	0.0111	0.0168	2,13,17
	22.0	6.9	4.8	—	0.6	—	60	45	127	91	125	—	0.30	0.03	0.03	0.03	0.22	0.02	0.02	0.04	0.05	3.06	0.02	0.02	0.03	0.22	0.96	0.0005	0.0005	39
8219268	107.0	90.5	—	—	9.4	1.1	4550	4424	4702	4459	—	—	1.20	0.88	—	1.34	6.20	6.23	—	6.53	—	—	2.93	—	3.00	—	4.26	0.0153	0.0144	29,33
	3.2	0.9	—	—	0.1	—	75	—	—	233	—	—	0.19	0.02	—	0.17	0.36	0.01	—	0.35	—	—	0.01	—	0.30	—	0.96	0.0006	0.0006	
8228742	1139.0	1375.9	1036.9	—	62.0	4.8	6042	6048	6096	6165	6269	—	1.26	1.26	1.26	1.31	1.82	1.82	1.82	1.84	177.60	170.61	4.02	4.02	4.02	3.09	3.09	0.0114	0.0182	2,13,17
	34.0	13.8	10.4	—	0.6	—	60	56	206	92	108	—	0.18	0.02	0.02	0.01	0.10	0.01	0.01	0.01	0.04	29.21	0.01	0.01	0.03	0.21	0.96	0.0005	0.0005	37
8379927	2645.0	2981.4	2364.9	—	120.0	10.6	5998	5939	6096	6011	6147	—	1.12	1.11	1.12	1.09	1.12	1.12	1.12	1.11	53.30	33.97	4.38	4.39	4.25	1.76	1.88	0.0129	0.0153	2,3,37
	79.3	29.8	23.6	—	1.0	—	108	—	—	148	155	—	0.17	0.02	0.02	0.03	0.06	0.01	0.01	0.02	0.02	2.86	0.01	0.01	0.21	0.11	0.04	0.0019	0.0027	40
8394589	2165.0	2547.2	1891.5	—	109.5	8.1	6111	6105	5974	6120	6114	—	0.90	1.03	0.99	0.94	1.11	1.16	1.15	1.12	128.99	110.21	4.30	4.31	3.98	5.08	3.93	0.0086	0.0121	2,17,39
	124.0	25.5	18.9	—	1.9	—	116	74	260	181	245	—	0.24	0.03	0.03	0.04	0.11	0.02	0.02	0.02	0.03	4.46	0.02	0.02	0.21	0.47	0.49	0.0013	0.0014	40
8524425	1063.0	1128.0	831.3	—	59.4	5.0	5634	5513	5515	5629	5751	—	1.13	1.09	1.07	1.00	1.81	1.82	1.82	1.73	179.25	174.45	3.97	3.95	3.98	7.62	7.92	0.0158	0.0218	2,13,17
	28.0	11.3	8.3	—	0.6	—	60	57	188	173	160	—	0.15	0.02	0.02	0.07	0.09	0.01	0.01	0.02	0.04	7.98	0.01	0.01	0.03	0.53	0.49	0.0008	0.0008	39
8561221	491.0	488.0	370.5	—	29.8	2.4	5245	5183	5374	5238	5705	—	1.56	1.01	1.05	1.55	3.19	2.82	2.84	3.18	286.71	276.87	3.62	3.55	3.61	5.09	5.09	0.0125	0.0118	13,25

Table A1: – continued from previous page

Star	$\nu_{\rm max}$	$\nu_{\rm min0}$	$\nu_{\rm min1}$	$\nu_{\rm min2}$	$\Delta\nu$	$\langle\delta\nu_{02}\rangle$	$T_{\rm eS}$	$T_{\rm eVK}$	$T_{\rm eBV}$	$T_{\rm sis0}$	$T_{\rm sis1}$	$T_{\rm sis2}$	$M_{\rm sca}$	$M_{\rm sis0}$	$M_{\rm sis1}$	$M_{\rm lit}$	$R_{\rm sca}$	$R_{\rm sis0}$	$R_{\rm sis1}$	$R_{\rm lit}$	$d_{\rm obs}$	$d_{\rm sis}$	$g_{\rm sca}$	$g_{\rm sis}$	$g_{\rm spc}$	$t_{\rm sis}$	$t_{\rm yil}$	$Z_{\rm s}$	Z_0	Ref
	μHz	μHz	μHz	μHz	μHz	μHz	K	K	K	K	K	K	$M_\odot$	$M_\odot$	$M_\odot$	$M_\odot$	$R_\odot$	$R_\odot$	$R_\odot$	$R_\odot$	pc	pc				Gyr	Gyr			
	5.0	4.9	3.7	—	0.1	—	60	62	199	118	79	—	0.10	0.01	0.01	0.13	0.08	0.01	0.01	0.18	0.08	4.13	0.01	0.01	0.03	0.24	0.49	0.0006	0.0006	
8694723	1402.0	1661.8	1261.7	—	74.9	5.4	6258	6230	6355	6116	6232	—	1.12	1.12	1.11	0.96	1.53	1.54	1.54	1.44	121.47	119.16	4.12	4.11	3.97	3.31	3.31	0.0080	0.0128	2,3,39
	42.1	16.6	12.6	—	0.8	—	117	36	137	105	117	—	0.18	0.02	0.02	0.03	0.09	0.01	0.01	0.02	0.03	5.53	0.01	0.01	0.21	0.23	0.49	0.0012	0.0012	40
8702606	664.0	688.7	554.5	—	39.7	3.5	5540	5396	5445	5489	6057	—	1.35	1.06	1.15	1.27	2.51	2.36	2.40	—	185.74	192.71	3.77	3.74	3.76	3.93	3.93	0.0121	0.0140	2,13,22
	16.0	6.9	5.5	—	0.5	—	60	70	192	171	108	—	0.19	0.02	0.02	—	0.14	0.01	0.01	—	0.06	4.27	0.01	0.01	0.03	0.31	0.49	0.0006	0.0006	
8760414	2333.0	2628.3	2041.6	—	117.1	5.6	5850	5925	5981	5960	6116	—	0.83	0.83	0.83	0.78	1.04	1.03	1.03	1.01	100.56	95.32	4.32	4.34	3.94	5.59	3.31	0.0042	0.0061	2,17,39
	121.0	26.3	20.4	—	0.4	—	166	59	194	222	226	—	0.18	0.01	0.01	0.01	0.08	—	—	0.01	0.02	10.92	0.01	0.01	0.26	0.20	0.17	0.0014	0.0019	40
9025370	2977.0	3246.7	2540.0	—	133.3	8.7	5704	5704	5630	5859	5930	—	1.00	1.00	1.00	0.84	1.01	1.01	1.01	0.96	87.42	64.55	4.42	4.43	—	5.51	4.73	0.0136	0.0175	2,17
	215.0	32.5	25.4	—	1.9	—	99	71	116	378	410	—	0.30	0.03	0.03	0.13	0.11	0.01	0.01	0.05	0.03	4.01	0.01	0.01	—	0.47	—	—	—	
9098294	2260.0	2494.9	1949.7	—	108.8	5.9	5766	5756	5930	5888	6036	—	0.99	0.99	1.00	1.00	1.16	1.15	1.15	1.15	125.45	117.49	4.31	4.31	4.27	7.20	6.38	0.0103	0.0152	2,17,39
	75.0	24.9	19.5	—	1.7	—	96	60	269	180	178	—	0.19	0.03	0.03	0.03	0.08	0.02	0.02	0.01	0.04	8.99	0.01	0.01	0.21	0.64	1.01	0.0016	0.0018	40
9139151	2566.0	2972.7	2270.0	—	116.7	10.1	6125	6116	6265	6119	6106	—	1.16	1.18	1.16	1.14	1.16	1.16	1.16	1.15	104.10	102.14	4.38	4.37	4.38	1.99	2.59	0.0153	0.0183	2,13,39
	77.0	29.7	22.7	—	2.1	—	60	53	214	121	162	—	0.20	0.03	0.03	0.03	0.08	0.02	0.02	0.01	0.02	6.19	0.02	0.02	0.03	0.20	0.27	0.0007	0.0016	
9139163	1672.0	2202.8	1619.8	1179.8	81.0	6.6	6400	6432	6395	6396	6405	6407	1.41	1.43	1.37	1.36	1.56	1.56	1.55	1.53	104.24	98.47	4.20	4.19	4.18	2.32	3.50	0.0160	0.0237	2,13,17
	58.0	22.0	16.2	11.8	1.1	—	60	36	128	47	106	141	0.24	0.03	0.03	0.03	0.10	0.01	0.01	0.02	0.03	4.57	0.01	0.01	0.03	0.19	0.98	0.0008	0.0019	39
9206432	1759.0	2289.7	1863.9	1355.8	84.3	7.7	6608	6524	6597	6382	6561	6567	1.39	1.35	1.41	1.40	1.50	1.50	1.52	1.48	151.76	145.79	4.23	4.22	4.23	1.57	2.39	0.0175	0.0241	2,13,17
	46.0	22.9	18.6	13.6	1.3	—	60	56	174	42	51	82	0.21	0.03	0.03	0.03	0.09	0.02	0.02	0.01	0.03	8.32	0.01	0.01	0.03	0.14	0.58	0.0009	0.0020	39
9410862	2235.0	2449.0	1912.1	—	107.0	7.8	6024	6024	6203	5854	5997	—	1.07	1.07	1.07	1.12	1.20	1.20	1.20	1.22	202.25	201.33	4.31	4.31	—	—	—	—	—	2,17
	67.0	24.5	19.1	—	1.9	—	100	118	—	175	172	—	0.20	0.03	0.03	0.11	0.09	0.02	0.02	0.05	0.05	9.11	0.02	0.02	—	—	—	—	—	
9574283	455.0	459.3	370.6	—	29.9	3.0	5120	—	—	5328	6044	—	1.16	0.89	0.99	1.07	2.88	2.72	2.77	—	354.86	359.10	3.59	3.55	—	4.05	4.05	0.0082	0.0078	2,17,22
	10.0	4.6	3.7	—	0.8	—	55	—	—	163	93	—	0.22	0.04	0.04	—	0.23	0.03	0.03	—	0.09	—	0.02	0.02	—	0.53	—	0.0001	0.0001	
9812850	1219.0	1558.0	1171.2	877.2	65.1	4.1	6258	6272	6393	6308	6395	6517	1.29	1.29	1.27	1.39	1.76	1.75	1.75	1.75	196.12	181.52	4.06	4.06	3.94	2.63	2.63	0.0103	0.0165	2,17,39
	60.0	15.6	11.7	8.8	1.1	—	97	51	223	89	131	139	0.31	0.03	0.03	0.05	0.16	0.02	0.02	0.02	0.06	20.68	0.02	0.02	0.21	0.25	—	0.0015	0.0015	40
9955598	3518.0	3530.0	2995.3	—	153.0	9.5	5264	5355	5480	5304	5894	—	0.83	0.83	0.89	0.89	0.87	0.87	0.88	0.88	69.38	62.04	4.48	4.50	4.29	8.30	4.95	0.0128	0.0166	2,29,39
	119.0	35.3	30.0	—	3.1	—	95	66	197	343	228	—	0.17	0.03	0.03	0.02	0.07	0.02	0.02	0.01	0.02	9.53	0.02	0.02	0.12	0.90	0.54	0.0017	0.0030	40
10018963	972.0	1168.7	866.0	—	55.2	5.1	6145	6125	6285	6130	6224	—	1.26	1.25	1.24	1.18	1.96	1.97	1.97	1.92	141.97	137.19	3.95	3.94	3.95	2.73	2.73	0.0097	0.0155	2,17,39
	32.0	11.7	8.7	—	0.5	—	112	43	131	103	120	—	0.20	0.02	0.02	0.03	0.12	0.01	0.01	0.02	0.03	4.33	0.01	0.01	0.21	0.17	0.54	0.0014	0.0014	40
10162436	1006.0	1370.4	977.0	671.1	55.5	3.6	6149	6155	6397	6397	6419	6413	1.37	1.42	1.35	1.23	2.00	2.00	1.98	1.90	137.89	133.39	3.97	3.97	3.95	2.34	2.34	0.0111	0.0177	2,17,39
	49.0	13.7	9.8	6.7	0.7	—	115	—	—	53	119	162	0.31	0.02	0.02	0.02	0.17	0.01	0.01	0.02	0.03	7.62	0.01	0.01	0.21	0.18	0.54	0.0017	0.0017	40
10355856	1330.0	1823.7	1308.8	—	68.1	4.7	6351	6326	6490	6427	6441	—	1.42	1.41	1.33	1.32	1.76	1.73	1.71	1.67	179.68	164.86	4.10	4.09	3.93	2.44	2.87	0.0103	0.0165	2,17,39
	42.0	18.2	13.1	—	0.7	—	118	47	189	32	86	—	0.23	0.02	0.02	0.03	0.11	0.01	0.01	0.01	0.05	13.32	0.01	0.01	0.21	0.16	0.99	0.0015	0.0031	40
10454113	2210.0	2594.3	2019.3	—	103.8	8.6	6120	6044	6179	6149	6238	—	1.18	1.18	1.18	1.19	1.26	1.25	1.25	1.25	112.52	83.48	4.31	4.31	4.31	2.35	2.57	0.0125	0.0165	2,13,17
	62.0	25.9	20.2	—	1.3	—	60	—	144	105	126	—	0.18	0.02	0.02	0.04	0.07	0.01	0.01	0.01	0.04	6.41	0.01	0.01	0.03	0.18	0.39	0.0006	0.0011	39
10516096	1700.0	—	—	—	84.6	—	5928	6006	5775	—	—	—	1.19	—	—	1.12	1.45	—	—	1.42	136.11	132.70	4.19	—	4.24	—	5.23	0.0128	0.0205	17,37,40
	30.0	—	—	—	1.1	—	95	67	188	—	—	—	0.15	—	—	0.03	0.07	—	—	0.03	0.04	—	0.01	—	0.21	—	1.19	0.0017	0.0019	
10644253	2819.0	3234.8	2623.1	—	123.2	9.8	6030	6046	5932	6103	6279	—	1.22	1.18	1.22	1.13	1.14	1.11	1.12	1.11	98.62	95.37	4.41	4.43	4.40	1.54	0.73	0.0154	0.0186	2,13,17
	131.0	32.3	26.2	—	2.7	—	60	60	160	182	191	—	0.30	0.04	0.04	0.05	0.11	0.02	0.02	0.02	0.03	5.16	0.02	0.02	0.03	0.18	0.08	0.0007	0.0023	39
10909629	839.0	—	843.7	—	49.6	3.0	6046	6046	6133	—	6479	—	1.23	—	1.34	1.36	2.09	—	2.13	2.17	479.22	393.02	3.89	3.91	—	—	—	—	—	2,17
	37.0	—	8.4	—	1.0	—	99	137	—	—	86	—	0.29	—	0.03	0.11	0.19	—	0.02	0.07	0.13	—	0.02	0.02	—	—	—	—	—	
10920273	1024.0	1103.1	826.6	—	57.1	4.9	5710	6189	6725	5707	5882	—	1.20	1.11	1.11	1.00	1.90	1.87	1.87	1.78	433.24	418.84	3.96	3.94	4.15	5.56	5.56	0.0131	0.0186	14,18,23
	64.0	11.0	8.3	—	0.6	—	75	216	—	319	299	—	0.30	0.02	0.02	0.04	0.17	0.01	0.01	0.02	0.18	11.96	0.01	0.01	0.08	0.38	—	0.0005	0.0005	
10963065	2132.0	2497.9	1885.3	—	102.6	7.3	6097	6116	6177	6130	6133	—	1.11	1.11	1.09	1.05	1.24	1.24	1.23	1.21	90.73	87.11	4.29	4.29	4.00	4.10	3.85	0.0097	0.0141	2,17,39
	62.0	25.0	18.9	—	1.0	—	130	35	143	110	144	—	0.18	0.02	0.02	0.02	0.07	0.01	0.01	0.01	0.02	10.70	0.01	0.01	0.21	0.27	0.55	0.0015	0.0018	40
11026764	895.0	945.6	698.3	—	50.2	4.5	5682	5374	5727	5605	5746	—	1.33	1.14	1.13	1.27	2.14	2.06	2.06	2.11	—	191.85	3.90	3.86	3.88	5.56	5.56	0.0142	0.0191	2,13,17
	29.0	9.5	7.0	—	0.6	—	60	34	155	205	188	—	0.21	0.02	0.02	0.06	0.13	0.01	0.01	0.03	—	4.67	0.01	0.01	0.03	0.42	0.55	0.0007	0.0007	39
11081729	1977.0	—	2391.0	1802.4	90.7	5.9	6630	6534	6637	—	6663	6743	1.48	—	1.48	1.26	1.46	—	1.42	1.38	135.67	135.88	4.28	4.30	4.25	1.52	—	0.0116	0.0186	2,13,17

Table A1: – continued from previous page

Star	$\nu_{\rm max}$	$\nu_{\rm min0}$	$\nu_{\rm min1}$	$\nu_{\rm min2}$	$\Delta\nu$	$\langle\delta\nu_{02}\rangle$	$T_{\rm eS}$	$T_{\rm eVK}$	$T_{\rm eBV}$	$T_{\rm sis0}$	$T_{\rm sis1}$	$T_{\rm sis2}$	$M_{\rm sca}$	$M_{\rm sis0}$	$M_{\rm sis1}$	$M_{\rm lit}$	$R_{\rm sca}$	$R_{\rm sis0}$	$R_{\rm sis1}$	$R_{\rm lit}$	$d_{\rm obs}$	$d_{\rm sis}$	$g_{\rm sca}$	$g_{\rm sis}$	$g_{\rm spc}$	$t_{\rm sis}$	$t_{\rm yil}$	$Z_{\rm s}$	Z_0	Ref
	μHz	μHz	μHz	μHz	μHz	μHz	K	K	K	K	K	K	$M_\odot$	$M_\odot$	$M_\odot$	$M_\odot$	$R_\odot$	$R_\odot$	$R_\odot$	$R_\odot$	pc	pc				Gyr	Gyr			
	84.0	—	23.9	18.0	1.4	—	60	55	207	—	24	55	0.30	—	0.03	0.03	0.11	—	0.02	0.02	0.04	—	0.01	0.01	0.03	0.14	—	0.0005	0.0057	39
11244118	1420.0	1526.8	1169.9	—	71.3	5.5	5745	5729	5491	5736	5868	—	1.33	1.20	1.21	1.10	1.69	1.65	1.65	1.59	159.72	166.56	4.10	4.09	4.09	5.32	5.95	0.0175	0.0280	2,13,17
	31.0	15.3	11.7	—	0.9	—	60	58	197	152	143	—	0.18	0.02	0.02	0.05	0.09	0.01	0.01	0.03	0.05	8.40	0.01	0.01	0.03	0.42	—	0.0009	0.0039	39
11253226	1638.0	2150.4	1684.6	1194.6	76.9	4.4	6410	6572	6768	6402	6520	6451	1.63	1.38	1.40	1.41	1.70	1.58	1.58	1.55	118.93	113.82	4.19	4.19	3.96	2.12	1.71	0.0106	0.0169	2,17,39
	48.0	21.5	16.8	11.9	1.0	—	125	38	156	41	68	118	0.28	0.03	0.03	0.05	0.11	0.01	0.01	0.02	0.05	5.24	0.01	0.01	0.21	0.17	0.50	0.0015	0.0022	40
11295426	2083.0	2233.4	1766.4	—	101.2	5.8	5793	5838	5712	5733	5969	—	1.04	1.04	1.06	1.08	1.24	1.24	1.24	1.24	148.84	137.78	4.27	4.28	4.28	7.16	9.69	0.0154	0.0213	27,29,46
	13.0	22.3	17.7	—	1.0	—	74	87	235	82	66	—	0.08	0.02	0.02	0.05	0.04	0.01	0.01	0.02	0.04	9.74	0.01	0.01	0.06	0.49	2.22	0.0006	0.0013	
11395018	834.0	875.3	685.2	—	47.3	4.2	5445	5517	5458	5566	5965	—	1.29	1.08	1.14	1.27	2.20	2.11	2.13	2.18	335.31	313.93	3.86	3.84	3.84	5.56	5.56	0.0156	0.0214	2,18,23
	50.0	8.8	6.9	—	0.5	—	85	101	376	345	264	—	0.31	0.02	0.02	0.04	0.19	0.01	0.01	0.02	0.08	3.01	0.01	0.01	0.12	0.38	2.22	0.0006	0.0006	
11414712	707.0	781.2	586.9	—	43.9	4.1	5635	5581	5563	5783	6063	—	1.11	1.09	1.11	1.26	2.20	2.23	2.24	2.34	128.52	122.14	3.80	3.78	3.80	4.94	4.94	0.0126	0.0155	2,13,17
	20.0	7.8	5.9	—	0.7	—	60	33	81	141	117	—	0.18	0.03	0.03	0.08	0.14	0.02	0.02	0.06	0.03	9.66	0.02	0.02	0.03	0.45	2.22	0.0006	0.0006	
11713510	1241.0	—	—	—	68.9	—	5893	5893	6055	—	—	—	1.05	—	—	1.00	1.60	—	—	1.57	252.43	261.22	4.05	—	—	—	—	—	—	17,37
	33.0	—	—	—	0.9	—	9	133	—	—	—	—	0.14	—	—	0.01	0.09	—	—	0.01	0.06	—	0.01	—	—	—	—	—	—	
11717120	585.0	583.7	434.3	—	37.8	4.2	5150	5034	5165	5263	5722	—	0.99	0.87	0.88	1.01	2.33	2.32	2.33	2.38	147.34	147.43	3.70	3.65	3.68	7.43	7.43	0.0093	0.0088	2,13,17
	8.0	5.8	4.3	—	0.9	—	60	42	140	128	87	—	0.15	0.04	0.04	0.10	0.16	0.02	0.02	0.11	0.04	3.90	0.02	0.02	0.03	0.89	—	0.0004	0.0004	
11771760	535.0	652.7	477.2	—	32.2	3.1	6142	—	—	6142	6246	—	1.81	1.47	1.46	1.55	3.16	2.97	2.97	3.00	676.56	—	3.70	3.66	—	—	—	—	—	2,17
	19.0	6.5	4.8	—	0.7	—	99	—	—	100	116	—	0.39	0.04	0.04	0.14	0.27	0.02	0.02	0.01	0.19	—	0.02	0.02	—	—	—	—	—	
11772920	3654.0	3709.5	—	—	157.4	8.7	5209	5371	5153	5401	—	—	0.82	0.83	—	—	0.85	0.85	—	—	72.88	64.52	4.49	—	4.34	—	9.12	0.0123	0.0169	2,40
	109.6	37.1	—	—	1.6	—	51	57	173	296	—	—	0.12	0.02	—	—	0.05	0.01	—	—	0.02	17.20	0.01	—	0.23	—	1.44	0.0017	0.0029	
11807274	1472.0	1678.7	1355.2	—	75.1	5.7	6225	6107	6365	6003	6284	—	1.29	1.22	1.29	1.26	1.60	1.59	1.61	1.58	263.62	261.73	4.14	4.13	4.13	3.29	3.50	0.0139	0.0214	16,29
	56.0	16.8	13.6	—	0.8	—	66	97	478	160	137	—	0.22	0.02	0.02	0.07	0.10	0.01	0.01	0.03	0.07	1.35	0.01	0.01	0.01	0.22	1.44	0.0007	0.0007	
12009504	1755.0	2003.2	1558.7	—	88.1	6.0	6099	6232	6022	6014	6168	—	1.14	1.13	1.14	1.12	1.39	1.39	1.39	1.38	143.22	122.40	4.21	4.21	4.00	4.46	5.41	0.0114	0.0170	2,17,39
	40.0	20.0	15.6	—	1.2	—	125	61	168	110	111	—	0.17	0.03	0.03	0.02	0.08	0.01	0.01	0.04	0.04	7.45	0.01	0.01	0.21	0.36	0.95	0.0017	0.0029	40
12069424	2143.0	2317.2	1802.2	—	103.4	5.8	5813	5790	5741	5782	5926	—	1.05	1.04	1.05	1.11	1.22	1.22	1.22	1.24	21.29	20.45	4.29	4.29	4.28	7.40	9.67	0.0152	0.0209	35,38,45
	64.3	23.2	18.0	—	1.0	—	18	—	—	189	181	—	0.14	0.02	0.02	0.02	0.06	0.01	0.01	0.01	0.01	1.36	0.01	0.01	0.02	0.51	2.41	0.0001	0.0004	
12069449	2485.0	2626.2	2114.5	—	116.7	6.6	5749	5745	5671	5661	5958	—	0.99	0.99	1.02	1.07	1.11	1.10	1.11	1.13	21.22	20.24	4.35	4.35	4.33	7.25	7.63	0.0144	0.0196	35,38,45
	74.5	26.3	21.1	—	1.2	—	17	—	—	219	181	—	0.13	0.02	0.02	0.02	0.06	0.01	0.01	0.01	—	1.12	0.01	0.01	0.02	0.49	1.36	0.0013	0.0015	
12258514	1440.0	1667.1	1251.8	—	74.5	4.9	5990	6017	6062	6052	6108	—	1.21	1.21	1.19	1.20	1.59	1.59	1.58	1.59	82.58	78.90	4.12	4.11	4.11	4.84	4.84	0.0141	0.0225	2,13,17
	43.0	16.7	12.5	—	0.8	—	60	—	—	121	141	—	0.18	0.02	0.02	0.08	0.09	0.01	0.01	0.04	0.02	2.78	0.01	0.01	0.03	0.35	1.36	0.0007	0.0007	39
12317678	1238.0	1681.9	1349.5	945.8	63.3	3.5	6401	6401	6760	6418	6588	6583	1.53	1.40	1.47	1.41	1.89	1.81	1.82	1.85	165.90	144.91	4.07	4.08	—	—	—	—	—	2,17
	40.0	16.8	13.5	9.5	0.8	—	99	39	153	36	48	87	0.26	0.02	0.02	0.13	0.12	0.01	0.01	0.06	0.06	6.00	0.01	0.01	—	—	—	—	—	
12508433	793.0	786.7	650.6	—	44.9	3.8	5134	5161	5062	5223	5959	—	1.22	0.96	1.06	1.17	2.23	2.11	2.15	2.20	155.18	159.97	3.83	3.80	3.50	6.34	6.34	0.0147	0.0151	2,17,40
	26.0	7.9	6.5	—	0.7	—	121	84	174	271	160	—	0.24	0.03	0.03	0.12	0.17	0.02	0.02	0.09	0.04	6.31	0.01	0.01	0.28	0.58	—	0.0021	0.0021	
2151	1000.0	1108.0	831.9	—	57.6	5.1	5790	5955	5762	5826	6021	—	1.10	1.11	1.11	1.08	1.83	1.87	1.87	1.81	—	7.08	3.95	3.94	3.84	5.05	5.05	0.0119	0.0176	8,11,12
	30.0	11.1	8.3	—	0.6	—	40	—	—	151	138	—	0.15	0.02	0.02	0.03	0.10	0.01	0.01	0.02	—	0.63	0.01	0.01	0.08	0.34	—	0.0004	0.0004	
43587	2228.0	2485.3	1965.2	—	106.4	6.0	5947	5835	5897	5941	6120	—	1.08	1.07	1.09	1.04	1.20	1.20	1.20	1.19	—	18.93	4.31	4.32	4.37	5.66	5.69	0.0131	0.0187	10,41
	15.0	24.9	19.7	—	1.1	—	17	79	64	68	60	—	0.07	0.02	0.02	0.01	0.03	0.01	0.01	0.04	—	1.38	0.01	0.01	0.04	0.38	1.09	0.0012	0.0015	
49385	1003.0	1154.8	881.3	—	56.3	4.1	6095	—	6241	5992	6181	—	1.27	1.26	1.27	1.25	1.94	1.96	1.97	1.94	75.41	71.64	3.97	3.96	4.00	4.01	4.01	0.0149	0.0239	19,20
	3.0	11.5	8.8	—	0.6	—	65	—	—	43	36	—	0.08	0.02	0.02	0.05	0.05	0.01	0.01	0.03	0.05	1.24	0.01	0.01	0.06	0.28	1.09	0.0009	0.0009	
49933	1760.0	—	2053.9	1670.8	86.1	2.2	6522	—	6922	—	6643	6768	1.29	—	1.31	1.28	1.45	—	1.41	1.46	29.62	29.23	4.23	4.26	4.00	2.05	1.02	0.0086	0.0137	1,34,47
	52.8	—	20.5	16.7	0.9	—	38	—	—	—	27	29	0.18	—	0.02	0.01	0.08	—	0.01	0.01	0.02	—	0.01	0.01	0.06	0.14	0.64	0.0008	0.0039	
52265	2074.0	2389.8	1808.0	—	98.1	8.2	6116	6096	6208	6079	6068	—	1.22	1.23	1.21	1.24	1.32	1.33	1.32	1.33	29.79	29.40	4.28	4.28	4.32	3.02	5.27	0.0173	0.0225	5,24,31
	20.0	23.9	18.1	—	1.0	—	110	—	—	64	76	—	0.12	0.02	0.02	0.02	0.05	0.01	0.01	0.02	0.01	1.66	0.01	0.01	0.20	0.21	0.86	0.0010	0.0033	
146233	3000.0	3202.1	2668.7	—	133.4	10.5	5693	6146	5680	5741	6117	—	1.01	0.98	1.04	1.03	1.02	1.00	1.01	1.02	—	13.17	4.43	4.44	4.48	2.96	2.28	0.0125	0.0151	7,32,47
	90.0	32.0	26.7	—	1.3	—	108	—	—	214	164	—	0.16	0.02	0.02	0.01	0.06	0.01	0.01	0.01	—	0.64	0.01	0.01	0.06	0.20	0.24	0.0004	0.0007	
181420	1539.0	—	1674.1	—	75.6	6.7	6580	6529	6590	—	6589	—	1.44	—	1.44	1.30	1.64	—	1.63	1.61	50.00	48.35	4.17	4.17	4.09	1.51	1.68	0.0126	0.0201	6,28,44

Table A1: – continued from previous page

Star	$\nu_{\rm max}$	$\nu_{\rm min0}$	$\nu_{\rm min1}$	$\nu_{\rm min2}$	$\Delta\nu$	$\langle\delta\nu_{02}\rangle$	$T_{\rm eS}$	$T_{\rm eVK}$	$T_{\rm eBV}$	$T_{\rm sis0}$	$T_{\rm sis1}$	$T_{\rm sis2}$	$M_{\rm sca}$	$M_{\rm sis0}$	$M_{\rm sis1}$	$M_{\rm lit}$	$R_{\rm sca}$	$R_{\rm sis0}$	$R_{\rm sis1}$	$R_{\rm lit}$	$d_{\rm obs}$	$d_{\rm sis}$	$g_{\rm sca}$	$g_{\rm sis}$	$g_{\rm spc}$	$t_{\rm sis}$	$t_{\rm yil}$	$Z_{\rm s}$	Z_0	Ref
	μHz	μHz	μHz	μHz	μHz	μHz	K	K	K	K	K	K	$M_\odot$	$M_\odot$	$M_\odot$	$M_\odot$	$R_\odot$	$R_\odot$	$R_\odot$	$R_\odot$	pc	pc				Gyr	Gyr			
	10.0	—	16.7	—	0.8	—	100	53	109	—	20	—	0.12	—	0.02	0.17	0.06	—	0.01	0.10	0.02	—	0.01	0.01	0.15	0.10	0.62	0.0006	0.0016	
181907	28.5	24.2	—	—	3.5	0.7	4725	4744	4758	4741	—	—	1.30	0.97	—	1.43	12.42	12.93	—	12.93	118.51	115.11	2.37	—	2.35	—	2.60	0.0112	0.0106	15,26,30
	0.7	0.2	—	—	0.1	—	65	—	—	132	—	—	0.20	0.03	—	0.23	0.76	0.01	—	0.44	0.10	0.52	0.01	—	0.04	—	0.62	0.0003	0.0003	
203608	2600.0	—	2488.0	—	120.3	6.7	6253	6165	6266	—	6371	—	1.08	—	1.06	0.93	1.10	—	1.08	1.06	—	9.77	4.39	4.40	4.36	3.08	1.05	0.0064	0.0102	42,43
	0.5	—	24.9	—	1.2	—	32	—	—	—	26	—	0.05	—	0.02	0.01	0.03	—	0.01	0.01	—	—	0.01	0.01	0.01	0.20	0.24	0.0002	0.0025	
Procyon A	1019.0	—	1129.7	739.4	55.2	2.5	6530	6544	6633	—	6599	6537	1.48	—	1.47	1.48	2.04	—	2.01	2.03	—	3.45	3.99	4.00	4.05	3.06	2.85	0.0134	0.0215	48,49,50
	11.0	—	11.3	7.4	0.5	—	90	—	—	—	21	42	0.13	—	0.02	0.01	0.07	—	0.01	0.01	—	—	0.01	0.01	0.04	0.20	659.15	—	—	51,52,53
$\odot$	3050.0	3256.6	2555.2	1879.5	136.0	9.8	5777	—	—	5742	5831	5840	1.00	0.99	0.99	1.00	1.00	0.99	0.99	1.00	—	—	4.44	4.44	4.44	4.66	4.26	0.0134	0.0167	
	49.9	32.6	25.6	18.8	0.1	—	20	—	—	141	137	148	0.06	0.01	0.01	0.01	0.02	—	—	0.01	—	—	0.01	0.01	0.01	0.14	0.41	0.0014	0.0014	